

4. PALEOCENE–EOCENE NANNOFOSSIL BIOSTRATIGRAPHY OF ODP LEG 183, KERGUELEN PLATEAU¹

James E. Arney² and Sherwood W. Wise Jr.²

ABSTRACT

Cores from Sites 1135, 1136, and 1138 of Ocean Drilling Program Leg 183 to the Kerguelen Plateau (KP) provide the most complete Paleocene and Eocene sections yet recovered from the southern Indian Ocean. These nannofossil-foraminifer oozes and chinks provide an opportunity to study southern high-latitude biostratigraphic and paleoceanographic events, which is the primary subject of this paper. In addition, a stable isotope profile was established across the Cretaceous/Tertiary (K/T) boundary at Site 1138.

An apparently complete K/T boundary was recovered at Site 1138 in terms of assemblage succession, isotopic signature, and reworking of older (Cretaceous) nannofossil taxa. There is a significant color change, a negative carbon isotope shift, and nannofossil turnover. The placement of the boundary based on these criteria, however, is not in agreement with the available shipboard paleomagnetic stratigraphy. We await shore-based paleomagnetic study to confirm or deny those preliminary results.

The Paleocene nannofossil assemblage is, in general, characteristic of the high latitudes with abundant *Chiasmolithus*, *Prinsius*, and *Toweius*. Placed in context with other Southern Ocean sites, the biogeography of *Hornibrookina* indicates the presence of some type of water mass boundary over the KP during the earliest Paleocene. This boundary disappeared by the late Paleocene, however, when there was an influx of warm-water discoasters, sphenoliths, and fasciculiths. This not only indicates that during much of the late Paleocene water temperatures were relatively equable, but preliminary floral and stable isotope analyses

¹Arney, J.E., and Wise, S.W., Jr., 2003. Paleocene–Eocene nannofossil biostratigraphy of ODP Leg 183, Kerguelen Plateau. In Frey, F.A., Coffin, M.F., Wallace, P.J., and Quilty, P.G. (Eds.), *Proc. ODP, Sci. Results*, 183, 1–59 [Online]. Available from World Wide Web: <http://www-odp.tamu.edu/publications/183_SR/VOLUME/CHAPTERS/014.PDF>. [Cited YYYY-MM-DD]

²Florida State University, 108 Carraway, Tallahassee FL 32306, USA. Correspondence author: arney@quartz.gly.fsu.edu

also indicate that a relatively complete record of the late Paleocene Thermal Maximum event was recovered at Site 1135. It was only at the beginning of the middle Eocene that water temperatures began to decline and the nannofossil assemblage became dominated by cool-water species while discoaster and sphenolith abundances and diversity were dramatically reduced.

One new taxonomic combination is proposed, *Heliolithus robustus* Arney, Ladner, and Wise.

INTRODUCTION

Ocean Drilling Program (ODP) Leg 183 Sites 1135, 1136, and 1138 are located on the Kerguelen Plateau (KP) in the southern Indian Ocean (Fig. F1). This feature, ~2500 km long and between 200 and 600 km wide, rises ~2–4 km above the surrounding abyssal plain. The present-day latitude of the plateau ranges from 46° to 64°S latitude with corresponding paleolatitudes of ~50° to 65°S at 63.6 Ma (Fig. F2). The main objectives of this leg were to study the emplacement and subsequent tectonic and paleoenvironmental history of this large igneous province (Shipboard Scientific Party, 2000a).

The KP began to form during the mid-Cretaceous as a subaerial volcanic edifice. It has since persisted as a major middepth oceanic topographic high. Following subsidence (Coffin, 1992), most of it remained above the calcite compensation depth until about Pliocene time. This has resulted in a record of environmental, oceanographic, and biotic changes from the Cretaceous to the Holocene along an 18° latitudinal transect across the Southern Ocean.

This paper examines the Paleocene–Eocene nannofossil biostratigraphy and some associated paleoceanographic events recorded in the stable isotope records at Sites 1135, 1136, and 1138 (Fig F1). Calcareous nannofossils are abundant to very abundant and, in general, moderately well preserved in all samples examined from all three sites. Preservation and individual nannofossil species abundance are recorded in Tables T1, T2, T3, and T4. All species considered in this report are listed in the “Appendix,” p. 22, and bibliographic references for most taxa are given in Perch-Nielsen (1985). Any taxa not cited therein are given in the references.

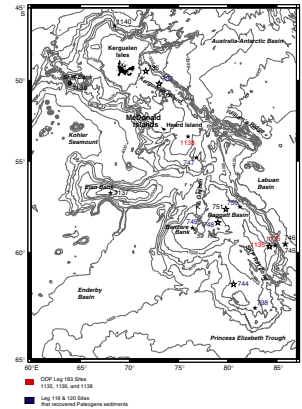
METHODS

Smear slides of raw sediment were examined at 1000× using standard light microscope techniques under crossed polarizers, transmitted light, phase-contrast light, and differential interference contrast light in order to estimate relative calcareous nannofossil abundance and preservation. A JSM-5900 scanning electron microscope was employed to take digital images for more precise species identification.

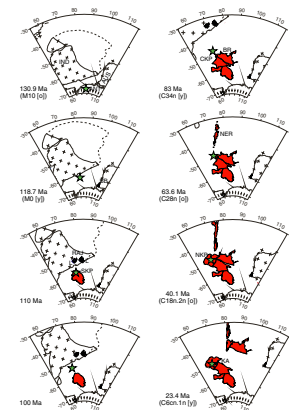
Estimates of overall nannofossil abundance were given the following letter codes:

- V = very abundant (>10 nannofossils/field of view).
- A = abundant (1–10 nannofossils/field of view).
- C = common (1 nannofossil/2–10 fields of view).
- F = few (1 nannofossil/>10–100 fields of view).
- R = rare (1 nannofossil/>100 fields of view).

F1. Bathymetry of the Kerguelen Plateau, p. 25.



F2. Emplacement and evolution of the Kerguelen Plateau, p. 26.



T1. Calcareous nannofossil taxa, Hole 1135A, p. 41.

T2. Calcareous nannofossil taxa, Hole 1136A, p. 42.

T3. Calcareous nannofossil taxa, Hole 1138A, p. 46

T4. Nannofossil counts across the K/T boundary, Site 1138, p. 47.

The average state of preservation of the nannofossil assemblage in each sample is designated as follows:

- VG = very good (no evidence of dissolution and/or overgrowth; no alteration of primary morphological characteristics, and specimens appear diaphanous; specimens are identifiable to the species level).
- G = good (little or no evidence of dissolution and/or overgrowth; primary morphological characteristics only slightly altered; specimens are identifiable to the species level).
- M = moderate (specimens exhibit some etching and/or overgrowth; primary morphological characteristics sometimes altered; however, most specimens are identifiable to the species level).
- P = poor (specimens are severely etched or exhibit overgrowth; primary morphological characteristics largely destroyed; fragmentation has occurred; specimens cannot be identified at the species and/or generic level).

Relative individual species abundance estimations follow the procedure of Hay (1970) and are indicated in the following manner:

- V = very abundant (>10–100 specimens per field of view),
- A = abundant (1–10 specimens per field of view).
- C = common (1 specimen per 2–10 fields of view).
- F = few (1 specimen per 11–100 fields of view).
- R = rare (1 specimen per 101–1000 fields of view).
- B = barren.

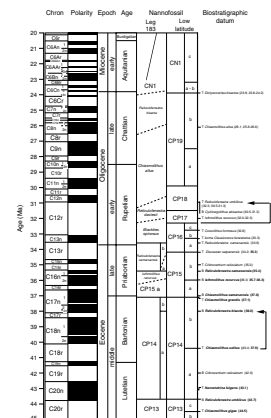
Oxygen and carbon isotopes were measured on bulk carbonate by grinding dried sediment to a homogenous powder and reacting ~60 µg of untreated sample in orthophosphoric acid at 70°C using a Finnigan-MAT Kiel III carbonate preparation device. Evolved CO₂ gas was measured online with a Finnigan-MAT 252 mass spectrometer at the University of Florida. All isotope results are reported in standard delta notation relative to Vienna Peedee belmenite (Coplen, 1996). Analytical precision for isotope analyses was ±0.03‰ for δ¹³C and ±0.06‰ for δ¹⁸O.

RESULTS

Biostratigraphy

The lower Paleocene is zoned using the high-latitude Antarctic zonal scheme of Wei and Pospichal (1991) (Fig. F3). On the other hand, the number-coded coccolith zonations compiled by Okada and Bukry (1980) and Martini (1971) are used in this report for the mid-Paleocene to Eocene sequences. Although the Okada and Bukry and Martini zonations were developed primarily for the low latitudes, the nannofossil assemblages in the mid-Paleocene and Eocene are, in general, diverse enough to allow application of these schemes. Nevertheless, some of the subzones could not be distinguished and some zones had to be combined, resulting in reduced biostratigraphic resolution.

F3. Paleocene–Eocene nannofossil biostratigraphic scheme, p. 27.



Site 1135

Site 1135 (59°42.0'S, 84°16.4'E), located on the southern Kerguelen Plateau (Shipboard Scientific Party, 2000b), was rotary cored in a water depth of 1567 m. It penetrated 526 m of upper Pliocene to Upper Cretaceous sediment composed almost entirely of pelagic calcareous ooze and chalk, including an expanded section (238 m thick) of mid-Paleocene to Eocene nannofossil ooze (Fig. F4). Such a section is not well represented in previous coring of high southern latitude sites; in addition, it is remarkably free of the chert that impeded drilling of Paleocene–Eocene sections on the KP during previous ODP Legs 119 and 120 (Schlich, Wise, et al., 1989; Barron, Larsen, et al., 1989). The Cretaceous/Tertiary (K/T) boundary is marked by a hiatus. Preservation is generally poor to moderate (Table T1).

Eocene

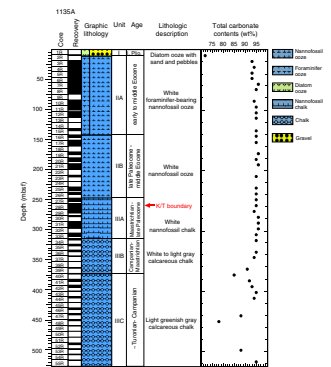
Sediments in Samples 183-1135A-3R-1, 131–133 cm (19.70 meters below seafloor [mbsf]), through 7R-6, 100–101 cm (64.60 mbsf), are placed in Subzone CP14a based on the overlap of *Reticulofenestra umbilica* and *Chiasmolithus solitus*. Diversity in this zone ranges from 20 to 25 species with abundant to common *Coccolithus pelagicus*, *C. solitus*, *Chiasmolithus expansus*, *Chiasmolithus* spp., *Reticulofenestra* spp., *Reticulofenestra samodurovii*, *R. umbilica*, *Sphenolithus moriformis*, and *Zygrhablithus bijugatus*.

Samples 183-1135A-7R-7, 25–26 cm (65.35 mbsf), through 17R-1, 25–26 cm (151.85 mbsf), are assigned to the combined *Discoaster subloadoensis*–*Nannotetrina quadrata* Zones (CP12–CP13). The assemblage is characterized by *C. pelagicus*, *C. solitus*, *C. expansus*, *Chiasmolithus* spp., *Neococcolithes dubius*, *Neococcolithes minutus*, *Reticulofenestra* spp., *R. samodurovii*, *R. umbilica*, *S. moriformis*, and *Z. bijugatus* throughout the interval. *Reticulofenestra onusta* is common to abundant in the upper part of this zone. Discoasters are few to rare in the upper part of the zone, but are few to common in the lower part. No attempt was made to determine the first occurrence (FO) of *Nannotetrina fulgens* (which separates Zone CP12 from CP13) because it was found only in a few samples and is too rare to be considered a useful datum at this site.

Samples 183-1135A-17R-1, 100–101 cm (152.60 mbsf), through 23R-CC (212 mbsf) are assigned to the combined *Discoaster lodoensis*–*Tribrachyatus orthostylus* Zone (CP11–CP10). The interval is normally defined as the FO of *D. lodoensis* to the FO of *D. sublodoensis*. Because of the poor preservation, however, the top of the zone is placed at the first common occurrence (FCO) of *D. sublodoensis*. *D. sublodoensis* was recorded in Table T1 below its FCO in a few samples down to Sample 183-1135A-21R-5, 100–101 cm (197 mbsf), but those identifications are questionable. The last occurrence (LO) of *T. orthostylus* is present in Sample 183-1135A-21R-1, 25–26 cm (188.61 mbsf), which places it in the middle of Zone CP11 (50.6 Ma). The assemblage contains abundant *C. pelagicus*, *Coccolithus formosus*, *C. solitus*, *N. dubius*, *N. minutus*, *Reticulofenestra* spp., *R. samodurovii*, *S. moriformis*, and *Z. bijugatus*.

Samples 183-1135A-25R-1, 25–26 cm (228.75 mbsf), through 25R-2, 100–101 cm (231 mbsf), are placed in the *Discoaster binodosus* Subzone (CP9b) based on the co-occurrence of *T. orthostylus* and *Tribrachyatus contortus*. This subzone marks the greatest diversification of sphenoliths at Site 1135; *S. moriformis*, *Sphenolithus primus*, *Sphenolithus radians*, and *Sphenolithus editus* are all common to abundant. The FOs of *C. expansus* and *Chiasmolithus grandis* are present in this subzone as well as the LO

F4. Site 1135 core summary, p. 29.



of *Chiasmolithus bidens*. The assemblage is characterized by abundant to common *Chiasmolithus* spp., *Toweius* spp., and *Z. bijugatus*. No *Reticulofenestra* spp. were observed in this zone.

Paleocene/Eocene Boundary

The Paleocene/Eocene boundary at Site 1135 is marked by an unconformity that is present between Samples 183-1135A-25R-3, 25–26 cm (231.75 mbsf), and 25R-2, 100–101 cm (231.0 mbsf), and spans Subzone CP9a (NP10). This unconformity was identified by the absence of the basal Eocene *Tribrachiatus bramlettei* and the presence of *T. contortus* and *T. orthostylus* as well as *Fasciculithus* spp. and *Prinsius bisulcus* in Sample 183-1135A-25R-2, 100–101 cm (231.0 mbsf). The *Fasciculithus* and *Prinsius* species are thought to be reworked. The FOs of *T. contortus* and *T. orthostylus* co-occur, indicating that the sample belongs to Subzone CP9b. Sample 183-1135A-25R-2, 25–26 cm (230.25 mbsf), contains the lower Eocene species *Discoaster barbadiensis* and *S. editus*.

Paleocene

The uppermost Paleocene *Discoaster multiradiatus* Zone (CP8) encompasses Samples 183-1135A-25R-3, 25–26 cm (231.75 mbsf), through 26R-CC (241.61 mbsf), which extends down to the FO of the marker *D. multiradiatus*. The assemblage is characterized by abundant *C. bidens*, *C. pelagicus*, *D. multiradiatus*, *Fasciculithus tympaniformis*, *P. bisulcus*, *S. primus*, *Toweius eminens*, and *Z. bijugatus*.

The *Discoaster nobilis* Zone (CP7) is missing. Either the marker is not present in this section or there is a hiatus that separates Sample 183-1135A-26R-CC (241.61 mbsf) from Sample 27R-1, 25–26 cm (247.95 mbsf), or the zone is present in the 6-m gap between samples.

The *Discoaster mohleri* Zone (CP6) is recorded in Sample 183-1135A-27R-1, 25–26 cm (247.95 mbsf), where the FO of *D. mohleri* is noted. The assemblage is characterized by abundant to common *Chiasmolithus danicus*, *C. pelagicus*, *F. tympaniformis*, *Fasciculithus magnicordis*, *Fasciculithus clinatus*, *Neochiastozygus perfectus*, *Neochiastozygus junctus*, *P. bisulcus*, *Prinsius martinii*, *S. primus*, *T. eminens*, and *Z. bijugatus*.

Similarly, Sample 183-1135A-27R-1, 100–101 cm (248.70 mbsf), is the only sample that contains the marker species *Heliolithus kleinpellii*; thus, it is assigned to the zone of that name (CP5). The assemblage is characterized by common to abundant *C. pelagicus*, *C. danicus*, *F. tympaniformis*, and *P. bisulcus*.

The *F. tympaniformis* Zone (CP4) is assigned to Samples 183-1135A-27R-2, 25–26 cm (249.45 mbsf), through 27R-CC (252.45 mbsf). The assemblage consists of abundant to common *C. pelagicus*, *Prinsius dimorphosus*, *Thoracosphaera* spp., *C. danicus*, *C. bidens*, *P. bisulcus*, *P. martinii*, *S. primus*, and *Toweius pertusus*.

For the lower Paleocene we used the high-latitude Antarctic zonation scheme of Wei and Pospichal (1991) (Fig. F3). The bottom of Zone CP4, defined as the FO of *F. tympaniformis*, roughly correlates to the middle of the *C. bidens* Zone (NA6) of Wei and Pospichal. The lower portion of the *C. bidens* Zone (NA6) and all of the *P. martinii* Zone (NA5) is missing. This hiatus is marked by the apparent FOs of *F. tympaniformis*, *P. martinii*, and *C. bidens* all in the same sample (183-1135A-27R-CC [252.45 mbsf]).

Sample 183-1135A-28R-1, 25–26 cm (257.55 mbsf), is assigned to the one-sample-long *C. danicus* Zone (NA4). The zone is based on the FO of *C. danicus* through the FO of *P. martinii*. The assemblage consists of *C. pelagicus*, *Cruciplacolithus tenuis*, *Placozygus sigmoides*, *P. dimorphosus*,

Thoracosphaera operculata, *Thoracosphaera* spp., *Cruciplacolithus primus*, and *C. danicus*.

The *C. tenuis* Subzone (NA3; CP1b) encompasses Samples 183-1135A-28R-1, 100–101 cm (258.30 mbsf), through 28R-2, 100–101 cm (259.80 mbsf), and is based on the FO of *C. tenuis* through the FO of *C. danicus*. The assemblage consists of abundant to common *C. pelagicus*, *C. tenuis*, *P. sigmoides*, *P. dimorphosus*, *T. operculata*, and *Thoracosphaera* spp., plus *Hornibrookina teuriensis*, which are few to common.

Site 1136

Site 1136 (59°39.1'S, 84°50.1'E), rotary cored in a water depth of 1931 m, is located ~30 km east of Site 1135 on the Southern Kerguelen Plateau (Shipboard Scientific Party, 2000c). At Site 1136, a 128-m-thick sedimentary section of middle Eocene to upper Albian sediments was recovered (Fig. F5). There is an expanded upper–lower to lower–middle Eocene section of calcareous ooze and chalk. Preservation is poor to moderate (Table T2).

Eocene

The topmost Sample 183-1136A-2R-1, 58–59 cm (5.28 mbsf), is placed in the *Discoaster bifax* Subzone (CP14a), as it contains the FO of *R. umbilica* plus *C. solitus*, whose LO marks the Subzone CP14a/CP4b boundary. The assemblage is characterized by abundant to common *C. solitus*, *C. pelagicus*, *N. dubius*, *N. minutus*, *Reticulofenestra* spp., and *Z. bijugatus*.

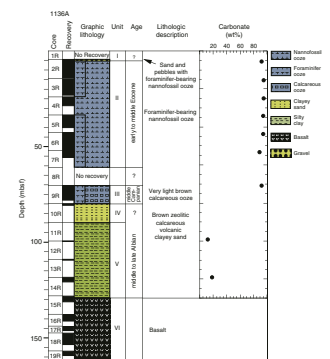
Samples 183-1136A-2R-2, 25–26 cm (6.45 mbsf), to 3R-2, 100–101 cm (16.90 mbsf), are placed in the *Chiasmolithus gigas* Subzone (CP13b), defined by the total range of *C. gigas*. The assemblage consists of common to abundant *C. expansus*, *C. solitus*, *C. formosus*, *C. pelagicus*, *N. dubius*, *N. minutus*, *R. onusta*, *R. samodurovii*, *Reticulofenestra* spp., *S. moriformis*, and *Z. bijugatus*.

The *Discoaster strictus* Subzone (CP13a) comprises Samples 183-1136A-3R-2, 100–101 cm (18.40 mbsf), through 4R-2, 100–101 cm (26.40 mbsf), and ranges from the FO of *N. fulgens* through the FO of *C. gigas*. The zone is characterized by common to abundant *C. expansus*, *C. solitus*, *C. formosus*, *C. pelagicus*, *N. dubius*, *N. minutus*, *R. onusta*, *R. samodurovii*, *Reticulofenestra* spp., *S. moriformis*, and *Z. bijugatus*. There is an increase in the abundance and diversity of discoasters overall as compared to the zones above. This may indicate that the oceans at this time were warmer than during the previous interval (Pospichal and Wise, 1990b)

The *D. sublodoensis* Zone (CP12) is assigned to Samples 183-1136A-4R-3, 25–27 cm (27.15 mbsf), through 5R-4, 25–26 cm (38.15 mbsf). Discoaster abundance increases in the assemblage, indicating warmer surface ocean temperatures during the early middle Eocene as compared with the late middle Eocene. The assemblage is characterized by common to abundant *C. expansus*, *C. grandis*, *C. solitus*, *C. formosus*, *C. pelagicus*, *Coronocylus prionion*, *D. binodosus*, *Discoaster kuepperi*, *D. lodoensis*, *Discoaster praebifax*, *N. dubius*, *N. minutus*, *R. samodurovii*, *Reticulofenestra* spp., *S. moriformis*, and *Z. bijugatus*.

Zones *D. lodoensis* (CP11) and *T. orthostylus* (CP10) are combined here because the marker species that separates them, *Toweius crassus*, is reported here out of its reported range. This combined zone encompasses Samples 183-1136A-5R-4, 100–101 cm (38.90 mbsf), to 6R-7, 25–26 cm (52.05 mbsf). Defined by the FO of *D. lodoensis* at its base and the FO of

F5. Site 1136 core summary, p. 30.



D. subladoensis at its top, this interval has common to abundant *C. bidens*, *C. solitus*, *C. pelagicus*, *D. binodosus*, *D. kuepperi*, *N. dubius*, *N. minutus*, *Reticulofenestra* spp., *S. moriformis*, *S. radians*, *Thoracosphaera* spp., *Toweius* spp., and *Z. bijugatus*. Also noted in this zone was the LO of *T. orthostylus* between Samples 183-1136A-6R-1, 100–101 cm (43.80 mbsf), and 6R-1, 25–26 cm (43.05 mbsf).

Samples 183-1136A-7R-1, 25–26 cm (52.35 mbsf), through 7R-2, 100–101 cm (54.60 mbsf), are assigned to the *D. binodosus* Subzone (CP9b). Defined as the FO of *T. orthostylus* (base) through the FO of *D. lodoensis* (top), this zone is relatively short and is characterized by abundant to common *C. bidens*, *C. consuetus*, *C. solitus*, *C. pelagicus*, *D. binodosus*, *D. kuepperi*, *N. dubius*, *S. moriformis*, *S. radians*, *T. crassus*, *Toweius* spp., and *Z. bijugatus*.

Site 1138

Site 1138 (53°33.1'S, 75°58.5'E), rotary cored in a water depth of 1141 m, is located on the central Kerguelen Plateau (Shipboard Scientific Party, 2000d). About 698 m of sediment was recovered, and the age ranges from Pleistocene to Late Cretaceous (Fig. F6). Six lithologic units are recognized at this site, one of which, Unit 3 (265.9–601.9 mbsf), was examined in this study. It consists of upper Oligocene to mid-Campian foraminifer-bearing chalk with scattered chert nodules in the lower section. There is a possibly complete K/T boundary section located in Core 183-1138A-52R (see “[Isotopic Analysis](#),” p. 10). This site provides an excellent chance to investigate environmental and biotic changes at high latitudes across this boundary (Table T3).

Eocene

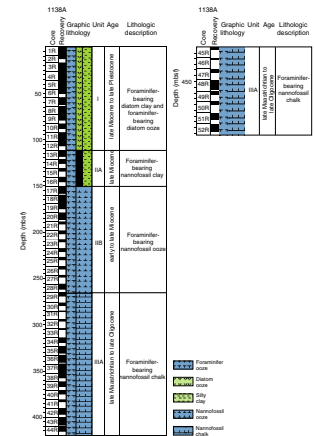
The *Isthmolithus recurvus* Subzone (CP15b) encompasses Samples 183-1138A-36R-5, 25–26 cm (339.25 mbsf), through 37R-2, 25–26 cm (344.34 mbsf). The FO of *I. recurvus* provides a well-documented datum for the base of the subzone (Wei and Wise, 1990; Wei, 1992). The top of the subzone is missing because of an unconformity between Samples 183-1138A-36R-5, 25–26 cm (339.25 mbsf), and 36R-4, 100–101 cm (337.75 mbsf). Sample 183-1138A-36R-5, 25–26 cm (339.25 mbsf), is of Eocene age, whereas Sample 36R-4, 100–101 cm (337.75 mbsf), is of early Oligocene age, based on the large number of *Chiasmolithus altus* relative to *Chiasmolithus oamaruensis* (Wei and Wise, 1990).

Subzone CP15b is characterized by abundant to common *C. oamaruensis*, *C. pelagicus*, *I. recurvus*, *Reticulofenestra* spp., *Reticulofenestra bisecta*, *R. umbilica*, and *Thoracosphaera* spp. The FO of *Reticulofenestra oamaruensis* is also noted in this subzone. Discoasters are almost completely absent. The only discoasters present are overgrown six-rayed forms that cannot be identified to species level.

Samples 183-1138A-37R-2, 100–101 cm (345.1 mbsf), through 37R-3, 100–101 cm (346.6 mbsf), are assigned to the *C. oamaruensis* Subzone, which extends from the LO of *C. grandis* to the FO of *I. recurvus*. The assemblage consists of abundant to common *C. oamaruensis*, *Coccolithus formosa*, *C. pelagicus*, *Reticulofenestra* spp., *R. bisecta*, *R. umbilica*, and *Thoracosphaera* spp. Other nannofossils include few to rare *Blackites spinosus*, *Discoaster* spp., *R. onusta*, *R. samodurovii*, *S. moriformis*, and *Z. bijugatus*.

Samples 183-1138A-37R-4, 25–26 cm (347.35 mbsf), through 37R-6, 100–101 cm (351.1 mbsf), belong to the *Discoaster saipanensis* Subzone (CP14b), defined by the LO of *C. solitus* at its base and the LO of *C. gran-*

F6. Site 1138 core summary, p. 31.



dis at the top. The FO of *R. bisecta* (38.0 Ma) is present within this subzone. The LO of *C. solitus* is reported above the FO of *R. bisecta* on the KP (this paper) and on the Falkland Plateau (Mostajo and Wise, 1983) (see “**Discussion**,” p. 11, for further detail). The assemblage consists of common to abundant *Chiasmolithus* spp., *C. formosus*, *C. pelagicus*, *Reticulofenestra* spp., *R. bisecta*, *R. samodurovii*, *R. umbilica*, *S. moriformis*, and *Thoracosphaera* spp.

The *D. bifax* Subzone (CP14a) is assigned to sediments of Samples 183-1138A-37R-CC (351.94 mbsf) through 43R-1, 100–101 cm (401.4 mbsf), based on the first common occurrence (FCO) of *R. umbilica* and presence of *C. solitus*. The top of the subzone is defined by the LO of *C. solitus*, and the base of the subzone is defined by the FO of *R. umbilica*. The base of this subzone is somewhat uncertain because of the nature of the species definition of *R. umbilica* (see “**Discussion**,” p. 11, for further details). The assemblage consists of abundant to common *C. solitus*, *C. formosus*, *C. pelagicus*, *Discoaster* spp., *Discoaster deflandrei*, five- and six-rayed *Discoaster* spp., *Reticulofenestra* spp., *R. onusta*, *R. samodurovii*, *R. umbilica*, *S. moriformis*, *Thoracosphaera* spp., and *Z. bijugatus*.

The *Coccolithus staurion* Subzone (CP13c) encompasses Samples 183-1138A-43R-2, 25–26 cm (402.15 mbsf), through 43R-4, 100–101 cm (405.9 mbsf). This subzone ranges from the LO of *C. gigas* to the FO of *R. umbilica*. The assemblage consists of abundant to common *C. solitus*, *C. formosus*, *C. pelagicus*, *Discoaster* spp., six-rayed *Discoaster* spp., *D. praebifax*, *Reticulofenestra* spp., *R. onusta*, *R. samodurovii*, *R. umbilica*, and *Z. bijugatus*.

Samples 183-1138A-43R-5, 25–26 cm (406.65 mbsf), through 45R-CC (422.8 mbsf) are assigned to the *C. gigas* Subzone (CP13b). This subzone is defined by the total range of *C. gigas*. The assemblage is made up of mostly abundant to common *C. expansus*, *C. grandis*, *C. solitus*, *C. formosus*, *C. pelagicus*, *Discoaster* spp., six-rayed *Discoaster* spp., *N. fulgens*, *N. dubius*, *Reticulofenestra* spp., *R. onusta*, *R. samodurovii*, and *Z. bijugatus*.

Sample 183-1138A-46R-1, 25–26 cm (429.55 mbsf), is assigned to the *Discoaster strictus* Subzone (CP13a). This subzone is defined at its base by the FO of *N. fulgens* and at its top by the FO of *C. gigas*. The assemblage consists of *C. solitus*, *C. formosus*, *C. pelagicus*, *N. dubius*, *Reticulofenestra* spp., *R. onusta*, *R. samodurovii*, and *Z. bijugatus*.

Samples 183-1138A-46R-CC (430.38 mbsf) through 47R-CC (441.92 mbsf) are assigned to the *D. sublodoensis* Zone (CP12). This zone extends from the FO of *D. sublodoensis* (base) to the FO of *N. fulgens* (top). The assemblage is characterized by abundant to common *C. solitus*, *C. formosus*, *C. pelagicus*, *Discoaster* spp., *D. binodosus*, *D. kuepperi*, *D. sublodoensis*, *Reticulofenestra* spp., and *Z. bijugatus*.

There is a hiatus between Samples 183-1138A-47R-CC (441.92 mbsf) and 48R-1, 25–26 cm (448.85 mbsf), that spans Zones CP10 and CP11. Samples 183-1138A-48R-1, 25–26 cm (448.85 mbsf), through 48R-1, 100–101 cm (449.6 mbsf), are assigned to the *D. binodosus* Subzone (CP9b). The assemblage is composed mostly of abundant to common *Chiasmolithus* spp., *C. pelagicus*, *D. kuepperi*, *Discoaster* spp., *Toweius* spp., *T. crassus*, and *Z. bijugatus*.

Paleocene/Eocene Boundary

The Paleocene/Eocene boundary is represented by a hiatus between Samples 183-1138A-48R-1, 100–101 cm (449.60 mbsf), and 48R-2, 25–26 cm (450.35 mbsf). The boundary is usually placed at the base of Subzone CP9a (NP10) based on the FO of *T. bramlettei*, which was not observed at this site. Sample 183-1138A-48R-1, 100–101 cm (449.60 mbsf),

contains the early Eocene species *T. orthostylus*, whose FO marks the base of Subzone CP9b (NP11). The next sample below, Sample 183-1138A-48R-2, 25–26 cm (450.35 mbsf), contains a Paleocene assemblage with *D. multiradiatus*, *F. tympaniformis*, and *P. bisulcus*.

Paleocene

Samples 183-1138A-48R-2, 25–26 cm (450.35 mbsf), through 48R-CC (457.3 mbsf) are assigned to the *D. multiradiatus* Zone, CP8 (NP9). The FO of *D. multiradiatus*, which is common throughout the zone, marks the Zone CP7/CP8 boundary. Diversity is relatively high, with abundant to common *C. bidens*, *C. pelagicus*, *Coccolithus* spp., *F. tympaniformis*, *P. bisulcus*, *S. primus*, *T. pertusus*, *Toweius tovae*, *Toweius* spp., and *Z. bijugatus*.

Samples 183-1138A-49R-1, 25–26 cm (458.45 mbsf), through 49R-1, 100–101 cm (459.20 mbsf), are assigned to the combined *D. nobilis*–*D. mohleri* Zone (CP7–CP6). This interval ranges from the FO of *D. mohleri* through the FO of *D. multiradiatus*. The FO of *D. nobilis* is normally used to separate Zone CP6 from CP7, but was not observed in this interval. The assemblage consists of *C. bidens*, *C. consuetus*, *Coccolithus* spp., *F. tympaniformis*, *Heliolithus* spp., *Heliolithus kleinpellii*, *P. bisulcus*, *T. eminens*, and *T. pertusus*.

As at Site 1135, the *H. kleinpellii* Zone (CP5) is represented in only one sample, 183-1138A-49R-2, 25–26 cm (459.95 mbsf). The zone is defined by the FO of *H. kleinpellii* at the base and the FO of *D. mohleri* at the top. The assemblage is similar to that at Site 1135, consisting of abundant to common *C. bidens*, *C. danicus*, *F. tympaniformis*, *H. kleinpellii*, *H. universus*, *P. sigmoides*, *P. bisulcus*, and *P. martinii*. The only noticeable difference is that Site 1138 has more common *Heliolithus* than Site 1135, perhaps a function of the lower latitude of Site 1135.

The *F. tympaniformis* Zone (CP4) spans Samples 183-1138A-49R-2, 100–101 cm (460.70 mbsf), through 49R-CC (461.69 mbsf). Defined by the FO of *F. tympaniformis* at the base and the FO of *H. kleinpellii* at the top, the assemblage is similar to that of Site 1135, consisting of *C. bidens*, *C. danicus*, *Coccolithus* spp., *F. magnicordis*, *F. tympaniformis*, *N. perfectus*, *P. sigmoides*, *P. bisulcus*, *P. martinii*, *Thoracosphaera* spp., and *T. pertusus*.

Samples 183-1138A-50R-1, 25–26 cm (467.75 mbsf), through 50R-CC (470.43 mbsf) are assigned to the *C. bidens* Zone (NA6) of the high-latitude Antarctic zonation scheme of Wei and Pospichal (1991), defined by the FO of *C. bidens* through the LO of *H. teuriensis*. It also encompasses the FO of *T. pertusus*, the FO of *P. bisulcus*, and the LO of *P. dimorphosus*. The assemblage consists of abundant to common *C. bidens*, *C. danicus*, *C. pelagicus*, *P. sigmoides*, *P. bisulcus*, *P. dimorphosus*, *P. martinii*, *T. operculata*, *Thoracosphaera* spp., and *T. pertusus*.

The *P. martinii* Zone (NA5), which was not present at Site 1135, consists of one sample, 183-1138A-51R-1, 25–26 cm (477.35 mbsf). The assemblage includes abundant to common *C. danicus*, *C. pelagicus*, *P. dimorphosus*, *P. martinii*, *T. operculata*, and *Thoracosphaera* spp.

The subjacent *C. danicus* Zone (NA4), represented by only one sample at Site 1135, here encompasses Samples 183-1138A-51R-1, 100–101 cm (478.10 mbsf), through 51R-4, 100–101 cm (482.60 mbsf). The assemblage consists of abundant to common *C. danicus*, *C. pelagicus*, *Cruciplacolithus edwardsii*, *P. dimorphosus*, *T. operculata*, and *Thoracosphaera* spp., with rare to few *Markalius inversus*, *Biscutum constans*, and reworked Cretaceous taxa. Site 1138 contrasts with Site 1135 by having

much fewer *H. teuriensis* and fewer *Chiasmolithus* and *Cruciplacolithus* throughout this zone.

Samples 183-1138A-52R-1, 3 cm (486.72 mbsf), through 52R-3, 4 cm (489.73 mbsf), are assigned to the *C. tenuis* Zone (NA3). The assemblage consists of abundant *C. pelagicus*, *C. tenuis*, *P. sigmoides*, *P. dimorphosus*, and reworked Cretaceous taxa. Few to rare *B. constans*, *C. edwardsii*, *C. primus*, *Cyclagelosphaera reinhardti*, *M. inversus*, *Neocrepidolithus cruciatus*, *N. fossus*, *Neocrepidolithus neocrassus*, and *Thoracosphaera* spp. are also present in this zone. In contrasting the assemblages of Site 1135 and Site 1138, we find that *H. teuriensis*, along with species of *Cruciplacolithus*, *P. sigmoides*, and *Thoracosphaera* spp., are all more abundant at the higher-latitude Site 1135.

The *H. teuriensis* Zone (NA2) is represented in Samples 183-1138A-52R-3, 10–11 cm (489.80 mbsf), through 52R-3, 29–29 cm (489.99 mbsf). The FO of *H. teuriensis* marks the base of the zone, and the top is defined by the FO of *C. tenuis*. The assemblage consists of common reworked Cretaceous taxa, few *P. sigmoides* and *Thoracosphaera* spp., and rare *B. constans*, *H. teuriensis*, *M. inversus*, *N. neocrassus*, and *Neocrepidolithus* spp.

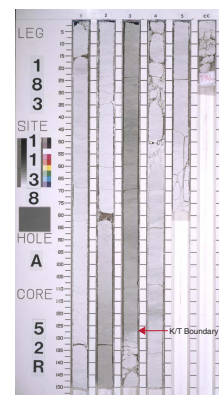
The *Biantholithus sparsus* Zone (NA1) encompasses Samples 183-1138A-52R-3, 40–42 cm (490.11 mbsf), through 52R-3, 127 cm (490.95 mbsf), which is unusually long for this zone (84 cm) relative to other Southern Ocean sites. The zone is defined as the FO of *B. sparsus* to the FO of *H. teuriensis*. The FO of *B. sparsus* is used to approximate the K/T boundary. This boundary was placed at Section 183-1138A-52R-3, 127 cm (490.95 mbsf), by the Shipboard Scientific Party (2000d) at a dramatic color change in Core 52R from a white chalk to a greenish clayey chalk (Fig. F7). The FO of *B. sparsus* was observed in Sample 183-1138A-52R-3, 70 cm (490.41 mbsf), some 57 cm above the color change. A stable isotopic analysis across this boundary supports this conclusion, although this is at odds with the conclusion from paleomagnetic stratigraphy (see “Discussion,” p. 11). The assemblage is characterized by abundant to common reworked Cretaceous taxa with rare to common *B. constans*, *M. inversus*, *N. neocrassus*, *P. sigmoides*, and *Thoracosphaera* spp.

Samples 183-1138A-52R-3, 129 cm (490.99 mbsf), through 52R-4, 10–11 cm (491.31 mbsf), just below the K/T boundary are assigned a late Maastrichtian age. Preservation is poor at the boundary, but as one moves down the section preservation improves significantly. The nannofossil assemblage is dominated by *Prediscosphaera stoveri*, which makes up ~30% of the assemblage (Table T4). Other taxa found were *Arkhangelskiella cymbiformis*, *Eiffellithus turriseiffelii*, *Kamptnerius magnificus*, *Nephrolithus frequens*, *Prediscosphaera cretacea*, and *Zygodiscus spiralis*.

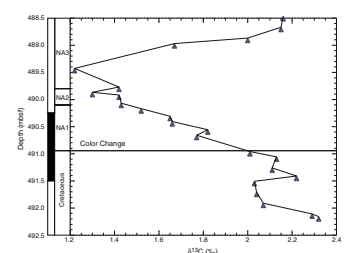
Isotopic Analysis

A bulk carbonate isotopic analysis across the K/T boundary in Core 183-1138A-52R is presented in Figure F8 along with some nannofossil datums. Samples 183-1138A-52R-4, 100–102 cm (492.21 mbsf), through 52R-4, 25–27 cm (491.46 mbsf), show an average $\delta^{13}\text{C}$ value of 2.25‰. The interpreted K/T boundary is placed at a color change at interval 183-1138A-52R-3, 127–128 cm (490.97 mbsf) (Fig. F7) (see “Discussion,” p. 11). $\delta^{13}\text{C}$ values decrease across the boundary to 1.75‰ and continue to decrease until a low of 1.20‰ in Sample 183-1138A-52R-2, 127–128 cm (489.48 mbsf), is reached in Zone NA3 (CP1b, NP2). The

F7. Core photo showing the K/T boundary, p. 32.



F8. Stable isotopic analysis across the K/T boundary, p. 33.



overall decrease in $\delta^{13}\text{C}$ is $\sim 1.05\text{‰}$ through this interval. Samples above interval 183-1138A-52R-2, 127–128 cm (489.48 mbsf), show a recovery of $\delta^{13}\text{C}$ back to previous values of $>2\text{‰}$ (see Table T5).

Linear Sedimentation Rates

Linear sedimentation rates, uncorrected for compaction, were calculated for the Paleogene section of each site and plotted with best-fit lines. Sedimentation rates for Hole 1135A are based on 13 nannofossil age estimates (Table T6). Sedimentation rates vary from 1.7 to 15.7 m/m.y. (Fig. F9). Apparently, low sedimentation rates for the upper and lower Paleocene are a product of hiatuses spanning Zones NA5, NA6, and CP7 (see Table T1). Linear sedimentation rates for Hole 1136A are based on seven nannofossil age estimates (Table T7). Sedimentation rates average 5.1 m/m.y. throughout the Eocene (Fig. F10). Linear sedimentation rates for Hole 1138A are based on 19 nannofossil age estimates (Table T8). Sedimentation rates vary from 1.7 to 9.2 m/m.y. (Fig. F11). Low sedimentation rates in the lower and upper Eocene can be attributed to hiatuses in those sections (Table T3).

At Sites 1135 and 1138, the lower Paleocene sedimentation rates are approximately the same (1.7 m/m.y.). This shows that sedimentation on the KP was similar in the southern and central areas. Both sites also show hiatuses in the lower upper Paleocene where marker species are missing or exceedingly rare.

Sites 1135, 1136, and 1138 all exhibit an unconformity at the Paleocene/Eocene boundary. At Sites 1135 and 1136, only the topmost section of the upper Paleocene and the lowermost Eocene is missing. At Site 1136, the unconformity below the Eocene spans the entire Paleocene and extends into the Cretaceous. Sediments of early to middle Eocene age are characterized by high sedimentation rates at all three sites (between 9 and 15 m/m.y.). Unfortunately, only Site 1138 has any upper Eocene sediment; therefore, we cannot compare the upper Eocene here with any other sites in this study (Fig. F12).

DISCUSSION

The KP provides a unique opportunity to study environmental, oceanographic, and biotic changes from the Cretaceous to the Holocene along an extended (18°) latitudinal north–south transect across an elevated Southern Ocean bathymetric feature. This possibility is not available anywhere else in Antarctic waters. Leg 183 has added considerably to the sediment recovery along this feature. However, since all sites were rotary cored during the leg, they are less than ideal for high-resolution paleoceanographic studies, as would be the case if hydraulic piston coring had been used. Nevertheless, the high sedimentation rates often recorded offset this handicap somewhat; therefore, it is useful to discuss some of the biostratigraphic and paleoenvironmental problems encountered. These are discussed in ascending stratigraphic order, beginning with the K/T Boundary.

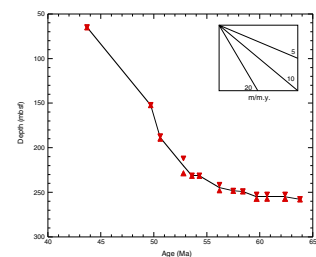
K/T Boundary Stable Isotopic Study

The K/T boundary at Site 1135 is represented by an unconformity that spans Zones NA1 and NA2 of Wei and Pospichal (1991). On the other hand, a complete boundary appears to have been recovered at

T5. Bulk carbonate isotopic values, Site 1138, p. 49.

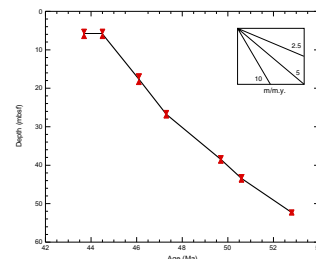
T6. Calcareous nannofossil events, Site 1135, p. 50.

F9. Age-depth plot, Hole 1135A, p. 34.



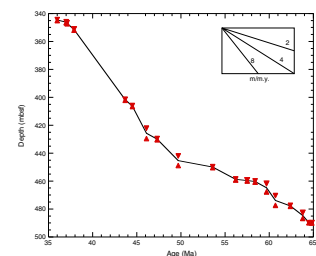
T7. Calcareous nannofossil events, Site 1136, p. 51.

F10. Age-depth plot, Hole 1136A, p. 35.



T8. Calcareous nannofossil events, Site 1138, p. 52.

F11. Age-depth plot, Hole 1138A, p. 36.



Site 1138, although the FO of *B. sparsus* (Sample 183-1138A-52R-3, 70 cm [490.4 mbsf]) occurs 57 cm above the dramatic color change (Sample 183-1138A-52R-3, 127 cm [490.97 mbsf]) at which the Shipboard Scientific Party placed the boundary. This is not surprising since *B. sparsus* is usually rare at most sites at which it is encountered (Table T4).

The initial shipboard (whole-core “pass through”) paleomagnetic stratigraphy, however, does not support this biostratigraphic placement of the K/T boundary at interval 183-1138A-52R-3, 127–128 cm (490.97 mbsf). Instead, the interval from 489 to 492 mbsf is interpreted as a paleomagnetic normal (Fig. F8) rather than the expected reversed interval (Shipboard Scientific Party, 2000d).

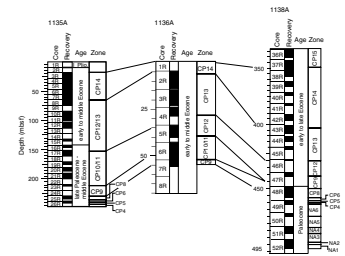
In contrast, however, our stable isotopic analysis reveals a 0.5‰ decrease in $\delta^{13}\text{C}$ across the interval at which the K/T boundary was placed (Fig. F8). This decrease of $\delta^{13}\text{C}$ is widely known to occur at the boundary (Pospichal, 1996a; Zachos et al., 1992; Stott and Kennett, 1990) and is similar to the amount measured at other Southern Ocean K/T sites. For example, at Site 750, a $\delta^{13}\text{C}$ decrease of $\sim 0.9\text{‰}$ (whole-rock sample) across the boundary was reported by Zachos et al. (1992). Site 690 on Maud Rise shows a decrease in $\delta^{13}\text{C}$ across the boundary in both benthic and planktonic foraminifers (Stott and Kennett, 1990). Site 527 (Walvis Ridge) also shows a decrease in $\delta^{13}\text{C}$ of $\sim 1\text{‰}$ across this boundary (Pospichal 1996a).

Some low-latitude sites, such as El Kef, Tunisia, show a greater shift in the carbon isotope values. Keller and Lindinger (1989) reported an isotopic shift of $\sim 2\text{‰}$ at the boundary. A 2‰ negative shift in the carbon isotopes is also reported at Agost, Spain (Smit, 1990) (Fig. F13) (see Pospichal, 1996a, for a summary of these sites). ODP Leg 171B sites (Blake Nose), on the other hand, show a decrease of only 1‰ across the boundary (Norris et al., 2001).

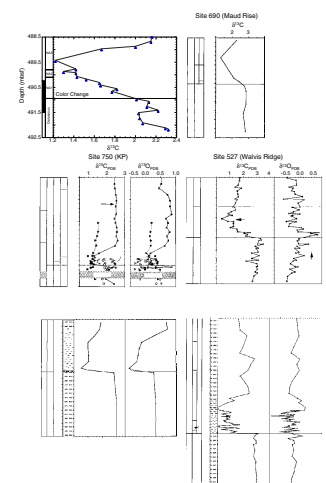
The overall pattern of a negative carbon isotope shift at the boundary indicates a global productivity collapse (Shackleton and Hall, 1984). The differing magnitudes of the carbon isotope shift at widely separated sites from around the world would seem to indicate different environmental responses to the crisis in different regions (Pospichal, 1996b). It has been suggested that the magnitude of the extinction may have varied significantly from the low to high latitudes (Keller, 1988), but this seems not to have been the case. Pospichal (1996b) and Pospichal and Wise (1990a) clearly demonstrated that the extinction event at the K/T boundary was just as severe in the high latitudes as it was in the low latitudes. The different values for the carbon isotopic shift, therefore, could result from taxonomic variations among the assemblages (mainly calcareous nannofossils) that contributed skeletal material to the fine-fraction carbonate used in isotopic analyses.

In addition, there is the problem of reworked Cretaceous taxa skewing the isotopic signal. This problem is especially acute at sites with heavy bioturbation. There, the more positive $\delta^{13}\text{C}$ Cretaceous taxa mix with the more negative $\delta^{13}\text{C}$ Danian taxa, resulting in carbon isotope values for the fine fraction somewhere in between the two end-member values. This mixing of Cretaceous and Danian taxa could also explain why $\delta^{13}\text{C}$ values reach their most negative values above the K/T boundary at approximately the Zone NA2/NA3 boundary at Sites 527, 738, 690, and 1138. In contrast, at El Kef and Agost, Spain, sites with little reworking of Cretaceous taxa, the $\delta^{13}\text{C}$ negative shift is greatest at the K/T boundary (Pospichal, 1996a).

F12. Graphic correlation of sites, p. 37.



F13. Carbon isotope curves, p. 38.



It could also be argued that the location of the most negative $\delta^{13}\text{C}$ values indicate the location of the K/T boundary. This assumes that the original carbon isotope event occurred at this point, but that it has been “smeared out” by subsequent bioturbation.

Berger and Heath (1968) proposed a vertical mixing model that suggests that the signal of an event would not be moved up or down as a result of bioturbation and reworking. If this was the case at Site 1138, we would expect that the isotope excursion would have to coincide with the sedimentation change that occurred, indicated by the color change.

According to the model, the darkest part of the core would represent the sediment change, and the lightening of the sediment color away from that level (both above and below) would be due to vertical mixing. In other words, the darkest sediment color in the sequence would coincide with the most negative point in the $\delta^{13}\text{C}$ excursion. This is clearly not the case, however, as we find that the more negative values of the isotope excursion are present well above this dark zone, almost at the point where sediment is returning to the background color. The offset between the darkest color and the minimum value in the isotope excursion is 0.65 m. The pattern is best explained by assuming an instantaneous event at the K/T boundary (490.97 mbsf) that produced both a maximum color change plus a maximum change in the $\delta^{13}\text{C}$ values. The latter does not coincide with the former, however, because reworking of Cretaceous sediment has diluted the isotope signal.

In short, we believe our placement of the K/T boundary is supported by the isotopic and nannofossil data. Not only is *B. sparsus* found in several samples within Zone NA1, but there is a greater relative number of *M. inversus* within that interval in contrast to the underlying Maastrichtian, as is characteristic of the earliest Danian in other boundary sections (e.g., Southern Ocean Site 690; see Pospichal and Wise, 1990a).

We cannot resolve at present, however, the discrepancy between the nannofossil and isotopic data on the one hand and the paleomagnetic results on the other. One can formulate several multiple working hypotheses, such as

1. The preliminary shipboard paleomagnetic measurements for Section 183-1138A-52R-3 provided a false reading.
2. Paleomagnetic Chron C29r is missing because of a hiatus; hence, the interval present where we place the boundary is actually Chron C30 or even C31n, as implied by Petrizzo (2001).
3. *B. sparsus* may actually range into the Maastrichtian, and therefore cannot be used to distinguish Cenozoic from Cretaceous strata.
4. The dark sediment color in Section 183-1138A-52R-3 may actually be unrelated to the K/T boundary event but rather related to the influx of clay minerals from tectonic activity and subaerial basement exposure at this time to the south at ODP Site 747 (Shipboard Scientific Party, 1989).

The first and most logical test to make relative to these hypotheses would be to confirm or deny the shipboard paleomagnetic data for Section 183-1138A-52R-3. This would require shore-based measurements on discrete samples from that section that have been subjected to more intense demagnetization than is done onboard ship. Such samples were not taken during the cruise because of routine curatorial restrictions placed on any sections suspected to have a complete K/T boundary. We

note that shore-based measurements have considerably altered the ship-board magnetic reversal stratigraphy originally suggested for the subjacent core, 183-1138A-53R (Antretter et al., this volume). Until such measurements are made on Section 183-1138A-52R-3, however, we can only speculate about the various hypotheses given above.

Lower Paleocene Biogeography

In the lower Paleocene, the high-latitude Antarctic zonation scheme developed by Wei and Pospichal (1991) was employed to achieve better biostratigraphic resolution in the study than that offered by either the Okada and Bukry or Martini zonations. Nevertheless, some zones are not present, notably NA4, NA5, and NA6 at Site 1135 and NA5 at Site 1138. Zoning the Paleocene proved difficult because of the absence or rarity of zonal index species. In particular, *D. nobilis*, *D. mohleri*, and *H. kleinpellii* are rare or absent; therefore, zonal boundaries using these datums are marked by uncertainties.

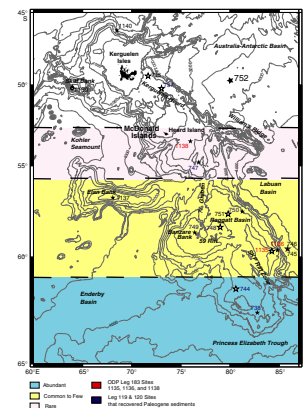
The lower Paleocene samples from Sites 1135 and 1138 do not show a *Hornibrookina* acme at the Zone NA2/NA3 boundary as reported by Pospichal and Wise (1990a) from Site 690 (Maud Rise) (see also Pospichal, 1996a). The abundance and distribution of the genus *Hornibrookina*, which evolved in the early Paleocene, can potentially be used to indicate a change in surface water conditions between Site 1135 at 59°S and Site 690 at 65°S at ~64.5 Ma.

Hornibrookina edwardsii constitutes 45% of the assemblage at Site 690 (Pospichal and Wise, 1990a), indicating ideal living conditions for that taxon. The ocean conditions were similar at Site 738 (62°S) at the southern tip of the KP, where *Hornibrookina* is “abundant” (Wei and Pospichal, 1991). These ocean conditions change, however, going toward the lower latitudes at Site 1135 (59°S), where *Hornibrookina* does not make up a significant portion of the assemblage. The highest abundance reached is “common” in one sample. Conditions continued to deteriorate for *Hornibrookina* at Site 1138 (53°S), where it is only “rare” in the assemblage. Even farther north at Site 752, Broken Ridge (then still part of the KP) (Fig. F2), Pospichal (1991) noted only one specimen of *Hornibrookina* just below Zone NA4. The distribution and abundance of *Hornibrookina* indicate oceanographic changes between Sites 738 and Site 1135 (Fig. F14). We interpret the data to indicate a water mass boundary or oceanographic front between those sites. The difference in the water masses could be due to temperature or possibly the amount of available nutrients. Further work needs to be done to better define these relationships.

Paleocene Sedimentation Rates and Core Recovery

The Paleocene section is marked by unconformities and/or condensed sections (Figs. F9, F10, F11). These condensed sections could reflect in part the moderate core recovery at Sites 1135 and 1138 (average recovery = 62.6% and 58.5%, respectively), which is similar to previous ODP legs to the KP. During Legs 119 and 120, condensed Paleocene sections were also recovered at Sites 738, 747, 748, and 750 (Wei and Thierstein, 1991; Aubry, 1992) and the core recovery was also poor (average = <50%) (Barron, Larsen, et al., 1989). It is likely, however, that several marker species used to define zonal boundaries in the Paleocene are not present or are sporadic in the section. This has hampered Paleocene biostratigraphic resolution on the KP. Nevertheless, Sites 1135 and

F14. Biogeography of genus *Hornibrookina*, p. 40.



1138 significantly increase the amount of biostratigraphic data available for the southern Indian Ocean through the Paleocene.

Late Paleocene Thermal Maximum

In the upper Paleocene Zone CP8 at Site 1135, the nannofossil data show an abundance switch from cool water-tolerant *Chiasmolithus* species to warm water-loving discoasters. This could indicate the presence of the late Paleocene Thermal Maximum in Core 183-1135A-25R. This possibility is currently being investigated using stable isotopic analysis, and those results will be reported elsewhere.

Eocene Core Recovery, Sedimentation Rates, and Hiatuses

The Eocene section is marked by variable core recovery. Some cores have >100% core recovery, whereas adjacent cores recovered <5%. This is due to chert stringers blocking the core barrel opening. Still, recovery was improved over previous ODP legs to the KP. During Legs 119 and 120, recovery averaged 55% and 40%, respectively, in the Eocene section (Barron, Larsen, et al., 1989; Schlich, Wise, et al., 1989), whereas during Leg 183 recovery averaged ~60% (Shipboard Scientific Party, 2000a) through thicker sections that contained less chert.

Sites 1135, 1136, and 1138 all have an unconformity at the Paleocene/Eocene boundary. The first unambiguously Eocene nannofossil recorded at each site was *T. orthostylus*, whose FO indicates the boundary between Subzones CP9a and CP9b (53.6 Ma). Overgrowth of *Tribrachiatulus* made identification at the species level difficult, but not impossible. No *T. bramlettei* was observed below the FO of *T. orthostylus*, thus indicating the unconformity at all three sites.

Generally, the lower Eocene to lower middle Eocene sections of Holes 1135A, 1136A, and 1138A have abundant and diverse assemblages of discoasters that include *D. barbadiensis*, *D. lodoensis*, *D. kuepperi*, and *D. sublodoensis*. The sphenolith group also reached its maximum diversity and abundance in the lower Eocene with *S. moriformis*, *S. primus*, *S. radians*, and *S. editus*. Nevertheless, for this report it was necessary to combine Zones CP10 and CP11 at all sites because of the sporadic nature of *T. crassus* (the FO of which marks the base of Zone CP11) and to combine Zones CP12 and CP13 at Site 1135 because of the sporadic presence of *N. fulgens* (whose FO marks the boundary between Zones CP12 and CP13).

There is an apparent change in the middle Eocene, where discoasters become few or absent and discoaster diversity becomes very low. In the middle Eocene, sphenoliths are represented by only one species, *S. moriformis*. At the same time that discoasters and sphenoliths were declining in overall abundance, *Chiasmolithus* and *Reticulofenestra* began to dominate the assemblage. This was especially true for the small reticulofenestrids during the early middle Eocene. This trend continued into the late middle Eocene, with the development of *R. onusta*, *R. samodurovii*, and *R. umbilica*. These changes in the nannofossil assemblage reflect the cooling trend in the middle Eocene reported by many other authors (Shackleton and Kennett, 1975; Shackleton and Hall, 1984; Oberhänsli et al., 1984; Pospichal and Wise, 1990b; Barrera and Huber, 1991; Aubry, 1992; Wei et al., 1992; Wise et al., 1992).

One of the biostratigraphic problems encountered in the middle Eocene was the Subzone CP13c/CP14a boundary. The FO of *R. umbilica*

is the datum used to define this boundary (Okada and Bukry, 1980). The Okada and Bukry zonation scheme was originally defined using low-latitude material. As drilling in higher latitudes progressed, it was noted that the Okada and Bukry zonal scheme, particularly the subzones, did not always readily apply. For instance, Applegate and Wise (1987) reported for offshore New Jersey that *R. umbilica* and *C. gigas* are present in the same samples and that their co-occurrence was not a result of contamination. Subzones CP13b and CP13c, therefore, could not be recognized in that region.

The present paper also reports *R. umbilica* and *C. gigas* in the same samples at Site 1138, but not at Sites 1136 and 1135 to the south. This could be due to the rarity of *C. gigas* at those sites. The co-occurrence of *R. umbilica* and *C. gigas* indicates that in higher latitudinal sections the FO of *R. umbilica* may be older than previously reported or that the LO of *C. gigas* is present later in the lower latitudes. For this reason the Zone CP13/CP14 boundary was approximated by the FCO of *R. umbilica*.

One other biostratigraphic question considered here is the extinction of *C. solitus*. In the lower latitudes, the LO of *C. solitus* is reported to occur below the FO of *R. bisecta* (Berggren et al., 1995). The LO of *C. solitus* at Site 1138, however, clearly occurs above the FO of *R. bisecta*. The same relationship was noted at Site 512 by Wise (1983) on the Falkland Plateau where *R. bisecta* was small, indicating the first evolutionary occurrence within a long section dominated by *C. solitus*. As that site was piston cored, there was no probability of contamination by caving of *C. solitus*.

Once again we have the problem of a marker species' range apparently being extended in the high latitudes. The alternative is that *R. bisecta* originated in the low/mid latitudes and subsequently migrated into the high latitudes after the appearance of *C. solitus*. This is considered less likely as both are cool-water taxa; hence, it is feasible that *C. solitus* might have persisted in the high latitudes after its disappearance at low latitudes.

The Leg 183 Shipboard Scientific Party placed the LO of *C. solitus* at 37.9 Ma for the high latitudes (see Wei and Wise, 1990) (Fig. F3), which is used in this paper. Berggren et al. (1995) assigned an age of 40.4 Ma to the LO *C. solitus* at low latitudes. This discrepancy in the age of the LO of *C. solitus* needs to be noted for the development of any chronology of events using the FO of *C. solitus* as a datum.

The upper Eocene was recovered on the KP only in Hole 1138A (Table T3). The overall assemblage reflects the trends of the late middle Eocene in that *Reticulofenestra* continues to dominate the assemblage along with cool-water *Chiasmolithus* species and *C. pelagicus*. The warm-water discoaster group declined in abundance to simple five- and six-rayed forms, now strongly overgrown. Sphenoliths continued to be represented by few to common *S. moriformis*, sometimes heavily overgrown.

CONCLUSIONS

The primary objective of this paper has been to summarize Paleocene to Eocene nannofossil biostratigraphy of Sites 1135, 1136, and 1138 on the KP and to compare the data with those from other sites on the KP.

1. The K/T boundary at Site 1138 appears to be complete in terms of assemblage succession, isotopic signature, and reworking of older (Cretaceous) nannofossil taxa. There is a significant color change, a negative carbon isotope shift, and nannofossil turnover. These three lines of evidence indicate that the boundary should be placed at Sample 183-1138A-52R-3, 127–128 cm (490.95 mbsf). These data compare favorably with other high-latitude sites, but this placement of the boundary is not in agreement with the current paleomagnetostratigraphy, which shows a paleomagnetic normal rather than reversed signature for this interval.
2. The biogeography of the genus *Hornibrookina* in the Southern Ocean indicates the presence of some type of water mass boundary over the KP during the very early Paleocene.
3. The application of an upper Paleocene–Eocene nannofossil biostratigraphy based on the Martini (1971) and Okada and Bukry (1980) zonal schemes is possible in the high latitudes, but significant problems arise in determining the absolute age of the FO and LO of some index taxa when comparing low-latitude to high-latitude sites. The Wei and Pospichal (1991) high-latitude scheme is more applicable for the lower Paleocene.
4. Discoasters and sphenoliths declined in abundance and diversity from the late Paleocene–early Eocene to the middle Eocene. This reflects the global cooling of the oceans during the middle Eocene.

SYSTEMATIC PALEONTOLOGY

(by J.E. Arney, B. Ladner, and S.W. Wise Jr.)

Genus *Heliolithus* Bramlette and Sullivan, 1961
Heliolithus robustus, n. comb.

Basionym: *Cycloolithus? robustus* Bramlette & Sullivan, 1961, p. 141, pl. 2, fig. 7a–7c.

Remarks: Wei (1998) has provided an excellent and thorough discussion (with synonymy) of this taxon, which he assigns to the genus *Ericsonia* Black, 1961, following the example of Perch-Nielsen (1977). The species consists of three cycles of elements, not unlike those in some species of *Heliolithus* (e.g., *H. universus* Wind and Wise, 1977). In *H. robustus*, however, the three cycles are tightly appressed. One could argue that the middle cycle corresponds to the outer distal shield in the genus *Coccolithus* (= *Ericsonia* of authors) and therefore should not birefringe in cross-polarized light. Because each cycle in a given specimen of *H. robustus* reaches about the same outer diameter, however, we have not been able to demonstrate such an optical effect under crossed nicols. Instead, each cycle appears to be entirely birefringent, a characteristic that fits the definition of *Heliolithus* rather than *Coccolithus* or *Ericsonia*.

ACKNOWLEDGMENTS

This paper is an excerpt from a thesis by James E. Arney, submitted in 2002, in partial fulfillment of the Master of Science degree at Florida State University. Some results have been presented in abstract by Arney and Wise (2001). We wish to thank all the participants of ODP Leg 183 for their contributions relevant to this paper. Special thanks go to Dr. Jason Curtis and the Stable Isotope Geochemistry Laboratory at the Uni-

versity of Florida under the direction of Professor David Hoddell. Without their help we would have been able to tell only half the story. We would like to thank the members of the Calcareous Nannofossil Laboratory at Florida State University for their helpful comments and assistance. Finally, we are indebted to Dr. James Pospichal, whose help has been invaluable to our understanding of the Southern Ocean. This research used samples and/or data provided by the Ocean Drilling Program (ODP). ODP is sponsored by the U.S. National Science Foundation (NSF) and participating countries under management of Joint Oceanographic Institutions (JOI), Inc. Funding for this research was provided by a USSAC grant to Dr. Sherwood W. Wise Jr.

REFERENCES

- Applegate, J.L., and Wise, S.W., Jr., 1987. Eocene calcareous nannofossils, Deep Sea Drilling Project Site 605, upper continental rise off New Jersey U.S.A. *In* van Hinte, J.E., Wise, S.W., Jr., et al., *Init. Repts. DSDP*, 93: Washington (U.S. Govt. Printing Office), 685–698.
- Arney, J., and Wise, S.W., Jr., 2001. Cretaceous/Tertiary boundary at ODP Site 1138 and paleobiogeography of calcareous nannofossil genus *Hornibrookina* in the early Paleocene. *Eos Trans. AGU*, 82:47S, Fall Meet. Suppl.
- Aubry, M.-P., 1992. Paleogene calcareous nannofossils from the Kerguelen Plateau, Leg 120. *In* Wise, S.W., Jr., Schlich, R., et al., *Proc. ODP, Sci. Results*, 120: College Station, TX (Ocean Drilling Program), 471–491.
- Barrera, E., and Huber, B.T., 1991. Paleogene and early Neogene oceanography of the southern Indian Ocean: Leg 119 foraminifer stable isotope results. *In* Barron, J., Larsen, B., et al., *Proc. ODP, Sci. Results*, 119: College Station, TX (Ocean Drilling Program), 693–717.
- Barron, J., Larsen, B., et al., 1989. *Proc. ODP, Init. Repts.*, 119: College Station, TX (Ocean Drilling Program).
- Berger, W.H., and Heath, G.R., 1968. Vertical mixing in pelagic sediments. *J. Mar. Res.*, 26:134–143.
- Berggren, W.A., Kent, D.V., Swisher, C.C., III, and Aubry, M.-P., 1995. A revised Cenozoic geochronology and chronostratigraphy. *In* Berggren, W.A., Kent, D.V., Aubry, M.-P., and Hardenbol, J. (Eds.), *Geochronology, Time Scales and Global Stratigraphic Correlation*. Spec. Publ.—SEPM (Soc. Sediment. Geol.), 54:129–212.
- Bramlette, M.N., and Sullivan, F.R., 1961. Coccolithophorids and related nannoplankton of the early Tertiary in California. *Micropaleontology*, 7:129–188.
- Coffin, M.F., 1992. Emplacement and subsidence of Indian Ocean plateaus and submarine ridges: synthesis of results from scientific drilling in the Indian Ocean. *Geophys. Monogr., Am. Geophys. Union*, 70:115–125.
- Coplen, T.B., 1996. Editorial: more uncertainty than necessary. *Paleoceanography*, 11:369–370.
- Hay, W.W., 1970. Calcareous nannofossils from cores recovered on Leg 4. *In* Bader, R.G., Gerard, R.D., et al., *Init. Repts. DSDP*, 4: Washington (U.S. Govt. Printing Office), 455–501.
- Keller, G., 1988. Extinction, survivorship and evolution of planktic foraminifers across the Cretaceous/Tertiary Boundary at El Kef, Tunisia. *Mar. Micropaleontol.*, 13:239–263.
- Keller, G., and Lindinger, M., 1989. Stable isotope, TOC and CaCO₃ record across the Cretaceous/Tertiary boundary at El Kef, Tunisia. *Palaeogeogr., Palaeoclimatol., Palaeoecol.*, 73:243–265.
- Martini, E., 1971. Standard Tertiary and Quaternary calcareous nannoplankton zonation. *In* Farinacci, A. (Ed.), *Proc. 2nd Int. Conf. Planktonic Microfossils Roma*: Rome (Ed. Tecnosci.), 2:739–785.
- Mostajo, E.L., and Wise, S.W., Jr., 1983. Correlation of Eocene–Oligocene calcareous nannofossil assemblages from piston cores taken near Deep Sea Drilling Sites 511 and 512, southwest Atlantic Ocean. *In* Ludwig, W.J., Krasheninnikov, V.A., et al., *Init. Repts. DSDP*, 71: Washington (U.S. Govt. Printing Office), 1171–1182.
- Norris, R.D., Kroon, D., Huber, B., and Erbacher, J., 2001. Cretaceous–Paleogene ocean and climate change in the subtropical North Atlantic. *In* Kroon, D., Norris, R.D., and Klaus, A. (Eds), *Proc. ODP, Sci. Results*, 171B [CD-ROM]. Available from: Ocean Drilling Program, Texas A&M University, College Station TX 77845-9547, USA, 1–22.
- Oberhänsli, H., McKenzie, J., Toumarkine, M., and Weissert, H., 1984. A paleoclimatic and paleoceanographic record of the Paleogene in the central South Atlantic (Leg

- 73, Sites 522, 523, and 524). In Hsü, K.J., LaBrecque, J.L., et al., *Init. Repts. DSDP*, 73: Washington (U.S. Govt. Printing Office), 737–747.
- Okada, H., and Bukry, D., 1980. Supplementary modification and introduction of code numbers to the low-latitude coccolith biostratigraphic zonation (Bukry, 1973; 1975). *Mar. Micropaleontol.*, 5:321–325.
- Perch-Nielsen, K., 1977. Albian to Pleistocene calcareous nannofossils from the western South Atlantic, DSDP Leg 39. In Supko, P.R., Perch-Nielsen, K., et al., *Init. Repts. DSDP*, 39: Washington (U.S. Govt. Printing Office), 699–823.
- , 1985. Cenozoic calcareous nannofossils. In Bolli, H.M., Saunders, J.B., and Perch-Nielsen, K. (Eds.), *Plankton Stratigraphy*: Cambridge (Cambridge Univ. Press), 427–554.
- Petrizzo, M.R., 2001. Late Cretaceous planktonic foraminifera from the Kerguelen Plateau (ODP Leg 183): new data to improve the Southern Oceans biozonation. *Cretaceous Res.*, 22:829–855.
- Pospichal, J.J., 1991. Calcareous nannofossils across Cretaceous/Tertiary boundary at Site 752, eastern Indian Ocean. In Weissel, J., Peirce, J., Taylor, E., Alt, J., et al., *Proc. ODP, Sci. Results*, 121: College Station, TX (Ocean Drilling Program), 395–414.
- , 1996a. Calcareous nannoplankton mass extinction at the Cretaceous/Tertiary boundary: an update. *Spec. Pap.—Geol. Soc. Am.*, 307:335–360.
- , 1996b. High latitude calcareous nannofossil changes at the Cretaceous/Tertiary boundary in the southern Indian Ocean. In Mokuilevsky, A., and Whatley, R. (Eds.), *Microfossils and Oceanic Environments*: Aberystwyth, UK (Univ. of Wales, Aberystwyth Press), 205–229.
- Pospichal, J.J., and Wise, S.W., Jr., 1990a. Calcareous nannofossils across the K/T boundary, ODP Hole 690C, Maud Rise, Weddell Sea. In Barker, P.F., Kennett, J.P., et al., *Proc. ODP, Sci. Results*, 113: College Station, TX (Ocean Drilling Program), 515–532.
- , 1990b. Paleocene to middle Eocene calcareous nannofossils of ODP Sites 689 and 690, Maud Rise, Weddell Sea. In Barker, P.F., Kennett, J.P., et al., *Proc. ODP, Sci. Results*, 113: College Station, TX (Ocean Drilling Program), 613–638.
- Schlich, R., Wise, S.W., Jr., et al., 1989. *Proc. ODP, Init. Repts.*, 120: College Station, TX (Ocean Drilling Program).
- Shackleton, N.J., and Hall, M.A., 1984. Carbon isotope data from Leg 74 sediments. In Moore, T.C., Jr., Rabinowitz, P.D., et al., *Init. Repts. DSDP*, 74: Washington (U.S. Govt. Printing Office), 613–619.
- Shackleton, N.J., and Kennett, J.P., 1975. Paleotemperature history of the Cenozoic and the initiation of Antarctic glaciation: oxygen and carbon isotope analyses in DSDP Sites 277, 279, and 281. In Kennett, J.P., Houtz, R.E., et al., *Init. Repts. DSDP*, 29: Washington (U.S. Govt. Printing Office), 743–755.
- Shipboard Scientific Party, 1989. Site 747. In Schlich, R., Wise, S.W., Jr., et al., *Proc. ODP, Init. Repts.*, 120: College Station, TX (Ocean Drilling Program), 89–156.
- , 2000a. Leg 183 summary: Kerguelen Plateau–Broken Ridge—a large igneous province. In Coffin, M.F., Frey, F.A., Wallace, P.J., et al., *Proc. ODP, Init. Repts.*, 183: College Station, TX (Ocean Drilling Program), 1–101.
- , 2000b. Site 1135. In Coffin, M.F., Frey, F.A., Wallace, P.J., et al., *Proc. ODP, Init. Repts.*, 183, 1–59 [CD-ROM]. Available from: Ocean Drilling Program, Texas A&M University, College Station, TX 77845-9547, U.S.A.
- , 2000c. Site 1136. In Coffin, M.F., Frey, F.A., Wallace, P.J., et al., *Proc. ODP, Init. Repts.*, 183, 1–96 [CD-ROM]. Available from: Ocean Drilling Program, Texas A&M University, College Station, TX 77845-9547, U.S.A.
- , 2000d. Site 1138. In Coffin, M.F., Frey, F.A., Wallace, P.J., et al., *Proc. ODP, Init. Repts.*, 183, 1–205 [CD-ROM]. Available from: Ocean Drilling Program, Texas A&M University, College Station, TX 77845-9547, U.S.A.
- Smit, J., 1990. Meteorite impact, extinctions and the Cretaceous–Tertiary boundary. *Geol. Mijnbouw*, 69:187–204.

- Stott, L.D., and Kennett, J.P., 1990. The paleoceanographic and paleoclimatic signature of the Cretaceous/Paleogene boundary in the Antarctic: stable isotopic results from ODP Leg 113. *In* Barker, P.F., Kennett, J.P., et al., *Proc. ODP, Sci. Results*, 113: College Station, TX (Ocean Drilling Program), 829–848.
- Varol, O., 1989. Eocene calcareous nannofossils from Sile (Northwest Turkey). *Rev. Esp. Micropaleontol.*, 21:273–320.
- Wei, W., 1992. Paleogene chronology of Southern Ocean drill holes: an update. *In* Kennett, J.P., and Warnke, D.A. (Eds.), *The Antarctic Paleoenvironment: A Perspective on Global Change*. *Antarct. Res. Ser.*, 56:75–96.
- , 1998. New calcareous nannofossil species and stratigraphic markers from the upper Paleocene. *J. Nannoplankton Res.*, 20:107–115.
- Wei, W., and Pospichal, J.J., 1991. Danian calcareous nannofossil succession at Site 738 in the southern Indian Ocean. *In* Barron, J., Larsen, B., et al., *Proc. ODP, Sci. Results*, 119: College Station, TX (Ocean Drilling Program), 495–512.
- Wei, W., and Thierstein, H.R., 1991. Upper Cretaceous and Cenozoic calcareous nannofossils of the Kerguelen Plateau (southern Indian Ocean) and Prydz Bay (East Antarctica). *In* Barron, J., Larsen, B., et al., *Proc. ODP, Sci. Results*, 119: College Station, TX (Ocean Drilling Program), 467–494.
- Wei, W., Villa, G., and Wise, S.W., Jr., 1992. Paleoceanographic implications of Eocene–Oligocene calcareous nannofossils from Sites 711 and 748 in the Indian Ocean. *In* Wise, S.W., Jr., Schlich, R., et al., *Proc. ODP, Sci. Results*, 120: College Station, TX (Ocean Drilling Program), 979–999.
- Wei, W., and Wise, S.W., 1989. *Discoaster praebifax* n. sp.—a possible ancestor of *Discoaster bifax* Bukry (Coccolithophoridae). *J. Paleontol.*, 63:10–14.
- Wei, W., and Wise, S.W., Jr., 1990. Biogeographic gradients of middle Eocene–Oligocene calcareous nannoplankton in the South Atlantic Ocean. *Palaeogeogr., Palaeoclimatol., Palaeoecol.*, 79:29–61.
- Wise, S.W., Jr., 1983. Mesozoic and Cenozoic calcareous nannofossils recovered by Deep Sea Drilling Project Leg 71 in the Falkland Plateau region, Southwest Atlantic Ocean. *In* Ludwig, W.J., Krasheninnikov, V.A., et al., *Init. Repts. DSDP*, 71 (Pt. 2): Washington (U.S. Govt. Printing Office), 481–550.
- Wise, S.W., Jr., Breza, J.R., Harwood, D.M., Wei, W., and Zachos, J.C., 1992. Paleogene glacial history of Antarctica in light of Leg 120 drilling results. *In* Wise, S.W., Jr., Schlich, R., et al., *Proc. ODP, Sci. Results*, 120: College Station, TX (Ocean Drilling Program), 1001–1030.
- Zachos, J.C., Aubry, M.-P., Berggren, W.A., Ehrendorfer, T., Heider, F., and Lohmann, K.C., 1992. Chemobiostratigraphy of the Cretaceous/Paleocene boundary at Site 750, southern Kerguelen Plateau. *In* Wise, S.W., Jr., Schlich, R., et al., *Proc. ODP, Sci. Results*, 120: College Station, TX (Ocean Drilling Program), 961–977.

APPENDIX

Calcareous Nannofossils Considered in This Paper

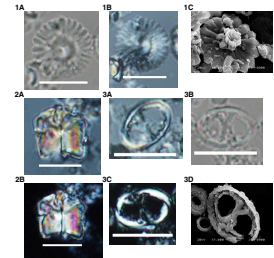
(In alphabetical order of generic epithets)

Examples of taxa are shown in Plates P1, P2, P3, P4, P5, P6, and P7.

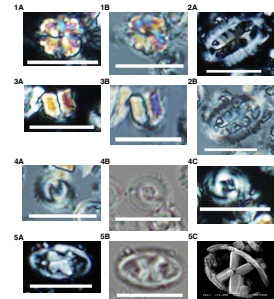
Cenozoic Taxa

- Amithalithina sigmundii* Pospichal and Wise, 1990
Biscutum constans (Gorka, 1957) Black in Black and Barnes, 1959
Biscutum spp.
Blackites spinosus (Deflandre and Fert, 1954) Hay and Towe, 1962
Braarudosphaera bigelowii (Gran and Braarud, 1935) Deflandre, 1947
Chiasmolithus bidens (Bramlette and Sullivan) Hay and Mohler, 1967
Chiasmolithus californicus (Sullivan, 1964) Hay and Mohler, 1967
Chiasmolithus consuetus (Bramlette and Sullivan) Hay and Mohler, 1967
Chiasmolithus danicus (Brotzen) Hay and Mohler, 1967
Chiasmolithus eograndis Perch-Nielsen, 1971
Chiasmolithus expansus (Bramlette and Sullivan) Gartner, 1970
Chiasmolithus grandis (Bramlette and Riedel) Radomski, 1968
Chiasmolithus oamaruensis (Deflandre, 1954) Hay, Mohler, and Wade, 1966
Chiasmolithus solitus (Bramlette and Sullivan) Locker, 1968
Chiasmolithus spp.
Chiasmolithus titus Gartner, 1970
Chiphragmalithus spp.
Coccolithus formosus (Kamptner) Wise, 1973
Coccolithus pelagicus (Wallich) Schiller, 1930
Coccolithus spp.
Coccolithus subpertusa Hay and Mohler, 1967
Coronocyclus nitescens (Kamptner, 1963) Bramlette and Wilcoxon, 1967
Cruciplacolithus edwardsii Romein, 1979
Cruciplacolithus frequens (Perch-Nielsen, 1977) Romein, 1979
Cruciplacolithus primus Perch-Nielsen, 1977
Cruciplacolithus spp.
Cruciplacolithus tenuis (Stradner) Hay and Mohler, 1967
Cyclicargolithus lumina Sullivan, 1965
Discoaster barbadiensis Tan, 1927
Discoaster bifax Bukry, 1971
Discoaster binodosus Martini, 1958
Discoaster deflandrei Bramlette and Riedel, 1954
Discoaster diastypus Bramlette and Sullivan, 1961
Discoaster kuepperi Stradner, 1959
Discoaster lenticularis Bramlette and Sullivan, 1961
Discoaster lodoensis Bramlette and Riedel, 1954
Discoaster megastypus Bramlette and Sullivan, 1961
Discoaster mohleri Bukry and Percival, 1971
Discoaster multiradiatus Bramlette and Riedel, 1954
Discoaster nobilis Martini, 1961
Discoaster nonradiatus Martini, 1961
Discoaster nonradiatus Klumpp, 1953
Discoaster praebifax Wei and Wise, 1989
Discoaster saipanensis Bramlette and Riedel, 1954
Discoaster spp.
Discoaster spp. (five ray)
Discoaster spp. (six ray)
Discoaster spp. (six ray) large
Discoaster sublodoensis Bramlette and Sullivan, 1961
Discoaster tani nodifer Bramlette and Riedel, 1954
Discoaster wemmelensis Achuthan and Stradner, 1969

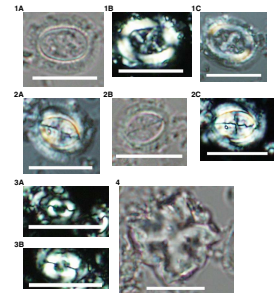
P1. Cores 183-1135A-25R and 26R, p. 53.



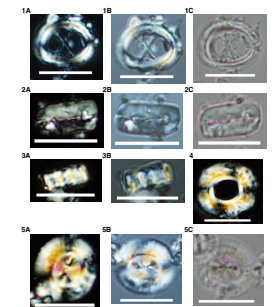
P2. Cores 183-1135A-25R and 26R and 183-1138A-44R, p. 54.



P3. Cores 183-1135A-27R and 183-1138A-44R, p. 55.

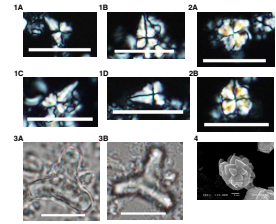


P4. Section 183-1138A-37R-1, p. 56.

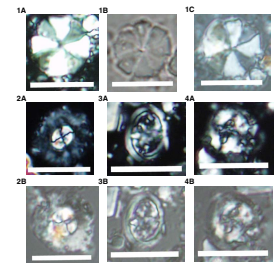


Ellipsolithus distichus (Bramlette and Sullivan) Sullivan, 1964
Ellipsolithus lajollaensis Bukry and Percival, 1971
Ellipsolithus macellus (Bramlette and Sullivan, 1961) Sullivan, 1964
Ellipsolithus spp.
Fasciculithus bobii Perch-Nielsen, 1971
Fasciculithus clinatus Bukry, 1971
Fasciculithus lilliana Perch-Nielsen, 1971
Fasciculithus magnicordis Romein, 1979
Fasciculithus magnus Bukry and Percival, 1971
Fasciculithus small (<4 µm)
Fasciculithus spp.
Fasciculithus thomasii Perch-Nielsen, 1971
Fasciculithus tympaniformis Hay and Mohler, 1967
Fasciculithus ulii Perch-Nielsen, 1971
Girgisia gammation Varol, 1989
Helicosphaera seminulum Bramlette and Sullivan, 1961
Helicosphaera spp.
Heliolithus cantabrigiae Perch-Nielsen, 1971
Heliolithus kleinpellii Sullivan, 1964
Heliolithus robustus (Bramlette and Sullivan, 1961) Arney, Ladner, and Wise in Arney and Wise, this paper
Hornibrookina teuriensis Edwards, 1973
Lapideacassis spp.
Markalius apertus Perch-Nielsen, 1979
Markalius astroporus (Stradner, 1963) Mohler and Hay in Hay et al., 1967
Markalius inversus (Deflandre) Bramlette and Martini, 1964
Nannotetrina fulgens Stradner, 1969
Neochiastozygus chiastus (Bramlette and Sullivan, 1961) Perch-Nielsen, 1971
Neochiastozygus concinnus (Martini, 1961) Perch-Nielsen, 1971
Neochiastozygus distentus (Bramlette and Sullivan, 1961) Perch-Nielsen, 1971
Neochiastozygus junctus (Bramlette and Sullivan, 1961) Perch-Nielsen, 1971
Neochiastozygus modestus Perch-Nielsen, 1971
Neochiastozygus perfectus Perch-Nielsen, 1971
Neochiastozygus saepes Perch-Nielsen, 1971
Neochiastozygus spp.
Neococcolithes dubius (Deflandre, 1954) Black, 1967
Neococcolithes minutus (Perch-Nielsen, 1967) Perch-Nielsen, 1971
Neococcolithes pediculatus (Perch-Nielsen, 1967) Perch-Nielsen, 1971
Neococcolithes spp.
Neorepidolithus fossus (Romein, 1977) Romein, 1979
Placozygus sigmoides (Bramlette and Sullivan, 1961) Romein, 1979
Pontosphaera spp. Lohmann, 1902
Prinsius bisulcus (Stradner, 1963) Hay and Mohler, 1967
Prinsius dimorphosus (Perch-Nielsen, 1969) Perch-Nielsen, 1977
Prinsius martinii (Perch-Nielsen, 1969) Haq, 1971
Prinsius spp.
Pseudotriquetrorhabdulus inversus (Bukry and Bramlette, 1969) Wise in Wise and Constans, 1976
Reticulofenestra daviesii Haq, 1971
Reticulofenestra dictyoda (Deflandre in Deflandre and Fert, 1954) Stradner in Stradner and Edwards, 1968
Reticulofenestra onusta (Perch-Nielsen) Wise, 1983
Reticulofenestra samodurovi (Hay, Mohler, and Wade, 1966) Roth, 1970
Reticulofenestra spp.
Reticulofenestra umbilica (Levin, 1965) Martini and Ritzkowski, 1968
Sphenolithus anarrhopus Bukry and Bramlette, 1969
Sphenolithus editus Perch-Nielsen in Perch-Nielsen et al., 1978
Sphenolithus moriformis (Bronnimann and Stradner, 1960) Bramlette and Wilcox, 1967
Sphenolithus primus Perch-Nielsen, 1971
Sphenolithus radians Deflandre in Grasse, 1952

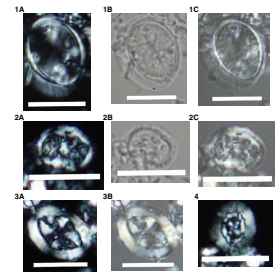
P5. Cores 183-1135A-20R, 22R, and 25R, p. 57.



P6. Sample 183-1138A-52R-3, 4 cm, p. 58.



P7. Sample 183-1138A-52R-3, 140–141 cm, p. 59.



Sphenolithus spiniger Bukry, 1971
Sphenolithus spp.
Thoracosphaera operculata Bramlette and Martini, 1964
Thoracosphaera spp.
Toweius? crassus (Bramlette and Sullivan, 1961) Perch-Nielsen, 1984
Toweius callosus Perch-Nielsen, 1971
Toweius craticulus Hay and Mohler, 1967
Toweius eminens (Bramlette and Sullivan, 1961) Romein, 1979
Toweius magnacrassus (Bukry, 1971) Romein, 1979
Toweius pertusus (Sullivan, 1965) Romein, 1979
Toweius spp.
Toweius tovae Perch-Nielsen, 1971
Tibrachiatus bramlettei (Bronnimann and Stradner, 1960) Proto Decima et al., 1975
Tibrachiatus orthostylus Shamrai, 1963
Zygodiscus spp.
Zygrhablithus bijugatus (Deflandre in Deflandre and Fert, 1954) Deflandre, 1959

Cretaceous Taxa

Acuturris scotus (Risatti, 1973) Wind and Wise in Wise and Wind, 1977
Ahmuellerella octoradiata (Gorka, 1957) Reinhardt, 1964
Arkhangelskiella cymbiformis Vekshina, 1959
Biscutum dissimilis Wind and Wise in Wise and Wind, 1977
Biscutum spp.
Chiastozygus amphipods (Bramlette and Martini, 1964) Gartner, 1968
Chiastozygus garrisonii Bukry, 1969
Chiastozygus spp.
Cribozentrum daniae Perch-Nielsen, 1973
Criboosphaerella ehrenbergii (Arkhangelsky) Deflandre in Piveteau, 1952
Eiffelithus spp.
Eiffelithus turriseiffelii (Deflandre in Deflandre and Fert) Reinhardt, 1965
Gartnerago spp.
Kamptnerius magnificus Deflandre, 1959
Lucianorhabdus cayeuxii Deflandre, 1959
Microrhabdulus decoratus Deflandre, 1959
Micula decussata Vekshina, 1959
Misceomarginatus pleniporus Wind and Wise in Wise and Wind, 1977
Monomarginatus quaternarius Wind and Wise in Wise and Wind, 1977
Nephrolithus frequens Gorka, 1957
Nephrolithus miniporus Gorka, 1957
Nephrolithus spp.
Prediscosphaera cretacea (Arkhangelsky) Gartner, 1968
Prediscosphaera spinosa (Bramlette and Martini, 1964) Gartner, 1968
Prediscosphaera spp.
Prediscosphaera stoveri (Perch-Nielsen) Shafik and Stradner, 1971
Reinhardtites anthophorus (Deflandre) Perch-Nielsen, 1968
Retacapsa crenulata Roth, 1970
Watznaueria barnesae (Black) Perch-Nielsen, 1968
Zygodiscus compactus Bukry, 1969
Zygodiscus spiralis Bramlette and Martini, 1964

Figure F1. Bathymetry of the Kerguelen Plateau. Leg 119, 120, and 183 drill sites that recovered igneous basement are indicated by solid stars; sites that bottomed in sediment are shown as open stars. Contour interval = 500 m (after Shipboard Scientific Party, 2000a, fig. F3).

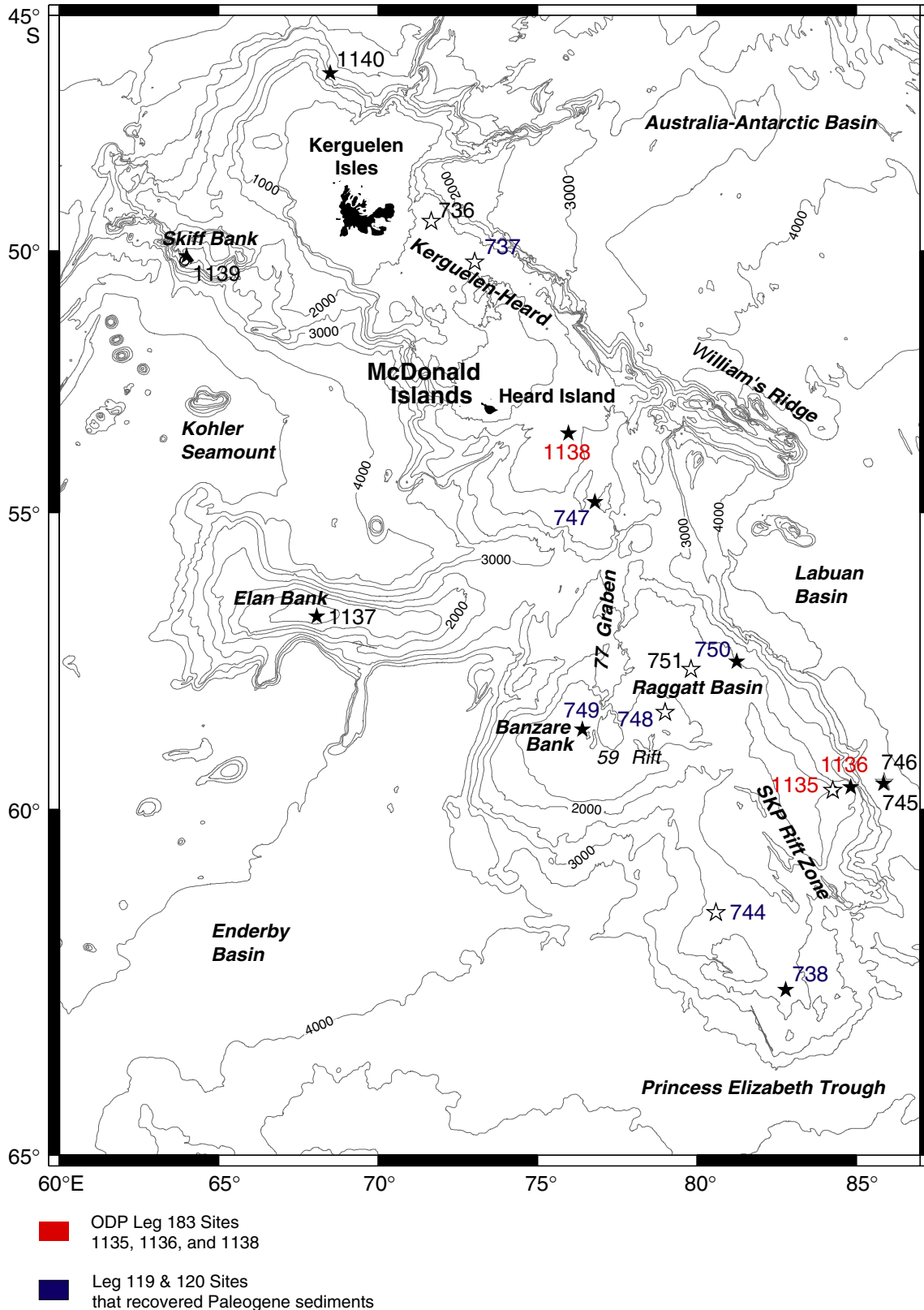


Figure F2. Emplacement and evolution of the Kerguelen Plateau from 130 Ma to present (after Shipboard Scientific Party, 2000a, fig. F2). CKP = central Kerguelen Plateau, BR = Broken Ridge, IND = India, ANT = Antarctica, AUS = Australia, BB = Bunbury Basalt, NER = Ninetyeast Ridge, RAJ = Rajmahal volcanic rocks, SKP = southern Kerguelen Plateau, NKP = northern Kerguelen Plateau, KA = Kerguelen archipelago.

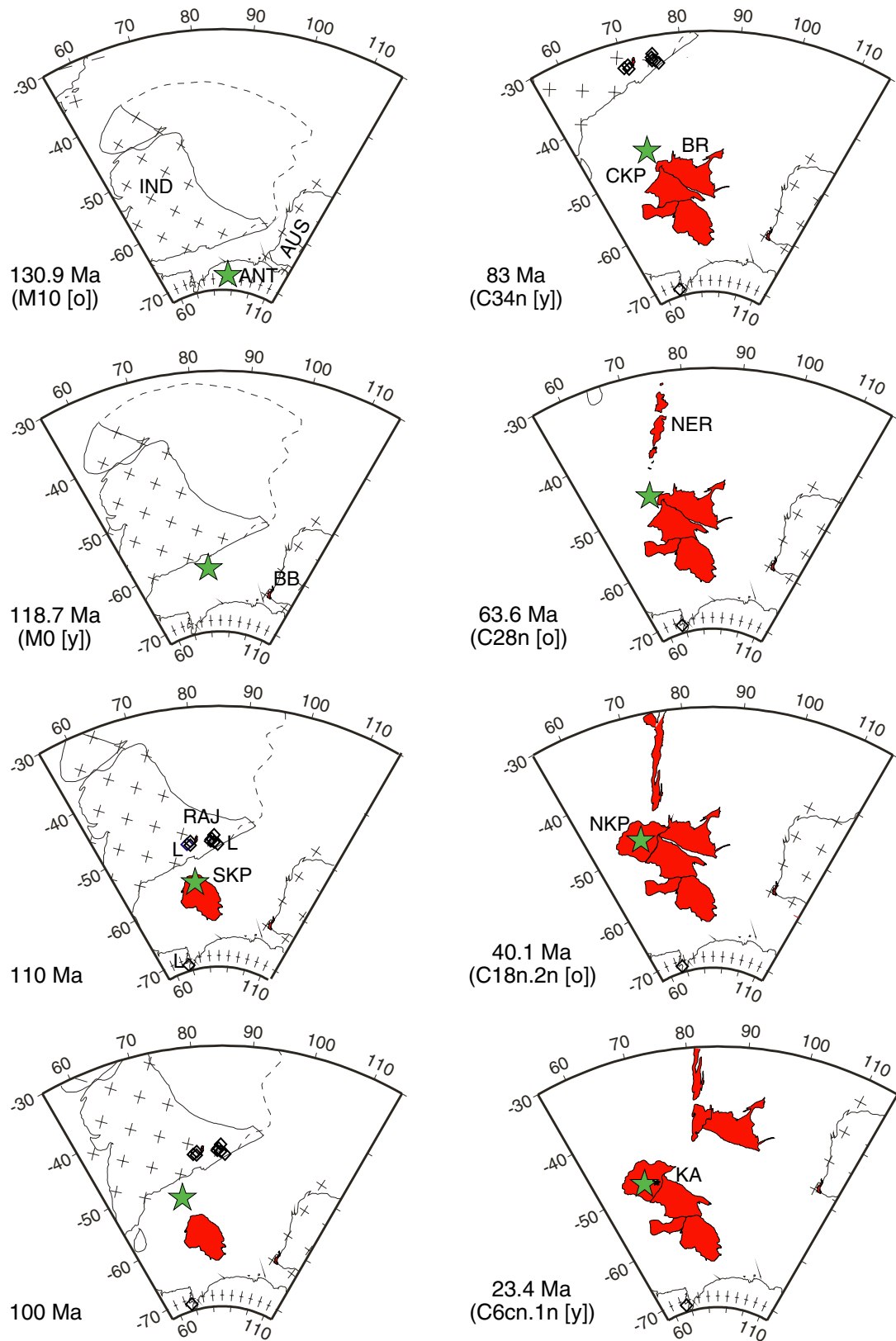


Figure F3. Paleocene–Eocene nannofossil biostratigraphic scheme of Okada and Bukry (1980) and the scheme of Wei and Pospichal (1991). Datum levels used in this report are in bold face (after Shipboard Scientific Party, 2000b, fig. F4). (Continued on next page.)

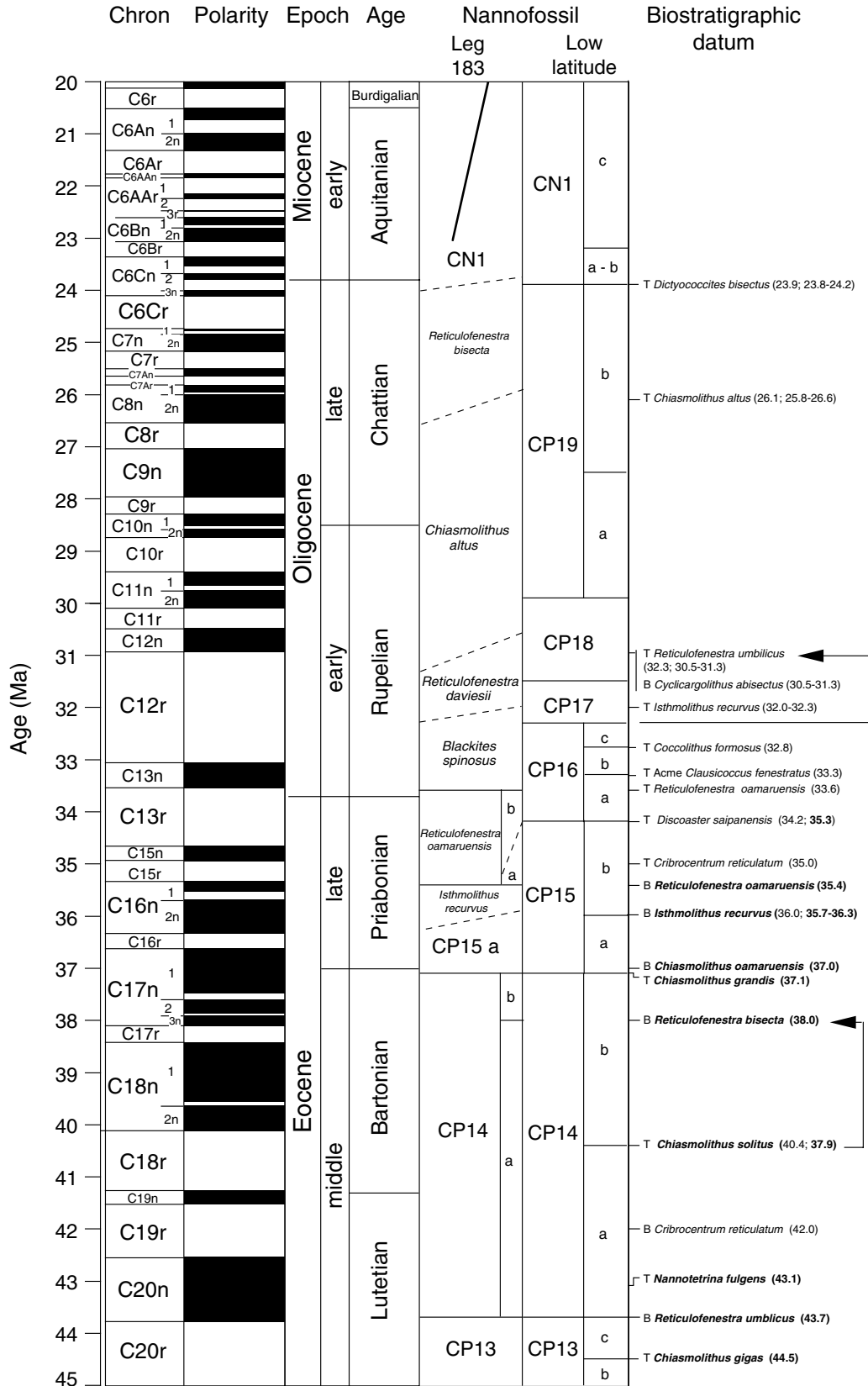


Figure F3 (continued).

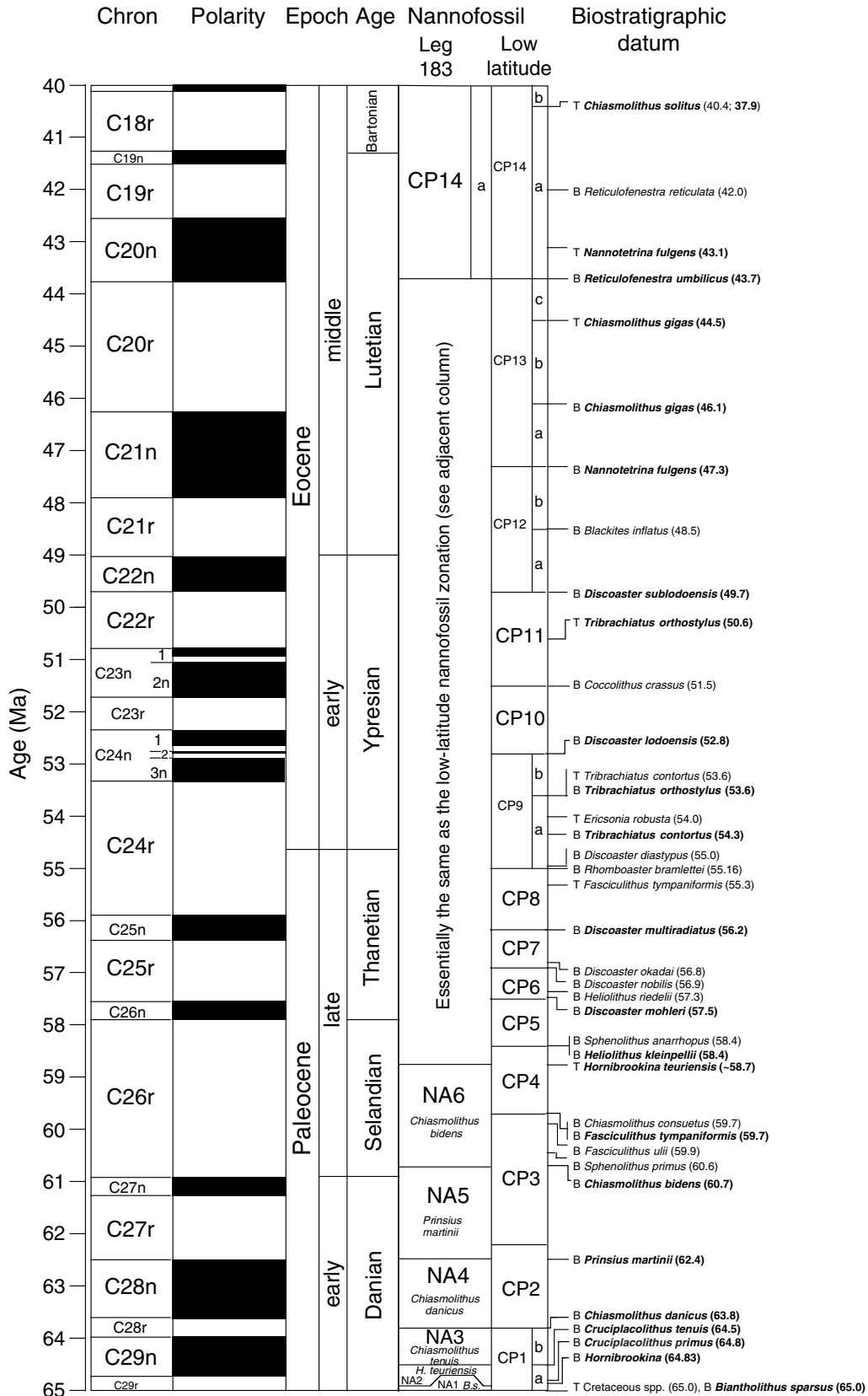


Figure F4. Site 1135 core summary (from Shipboard Scientific Party, 2000a, fig. F18).

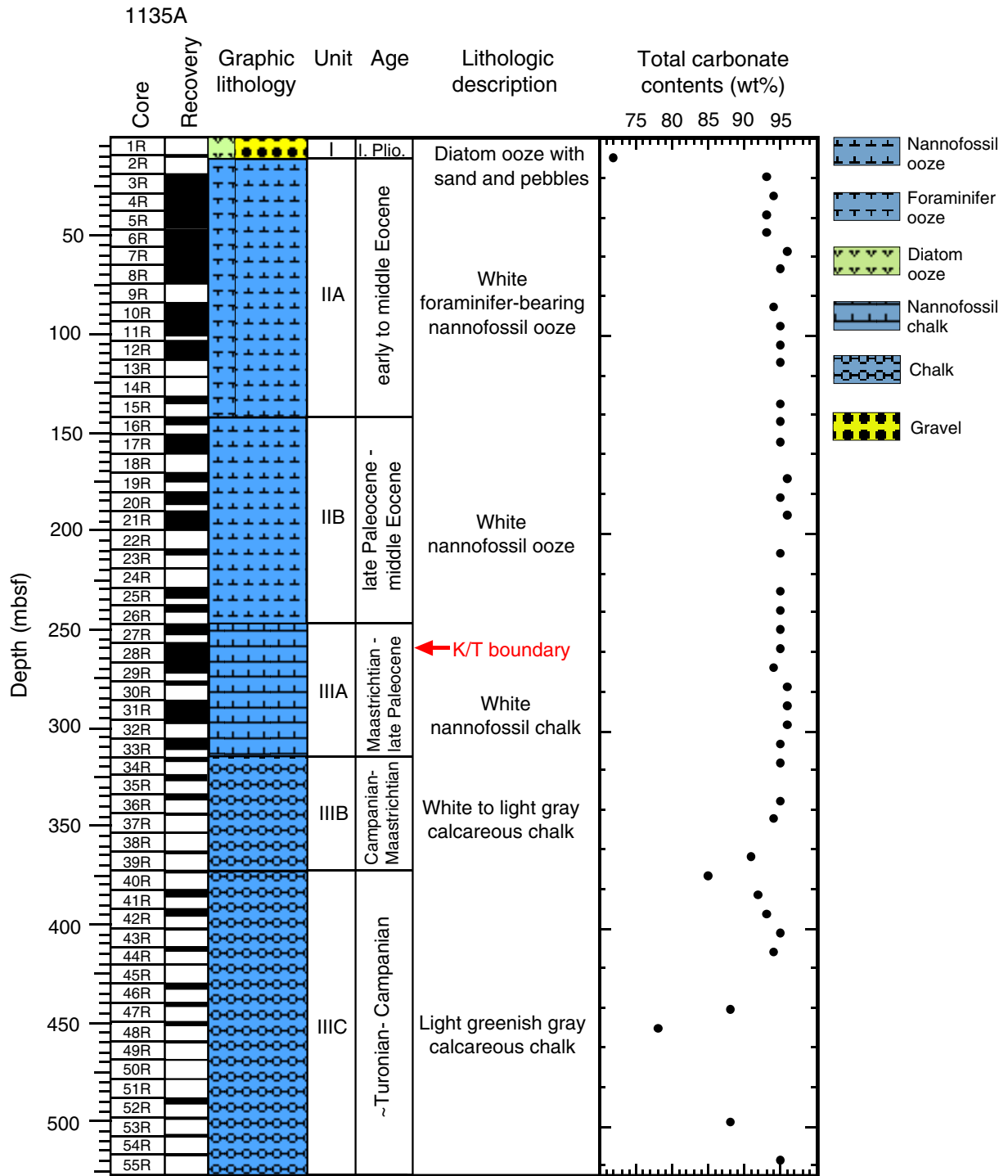


Figure F5. Site 1136 core summary (from Shipboard Scientific Party, 2000a, fig. F19).

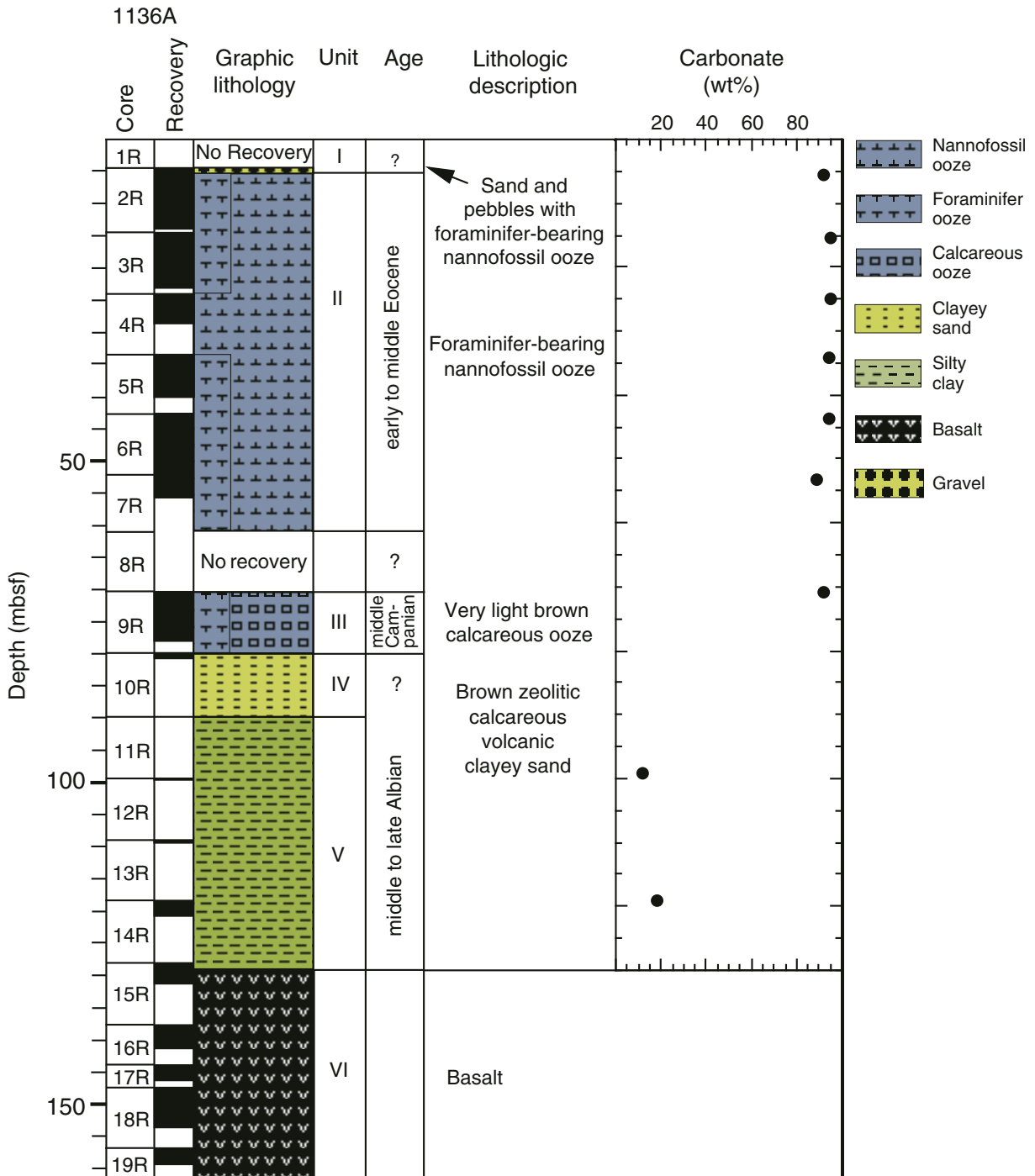


Figure F6. Site 1138 core summary (from Shipboard Scientific Party, 2000a, fig. F28).

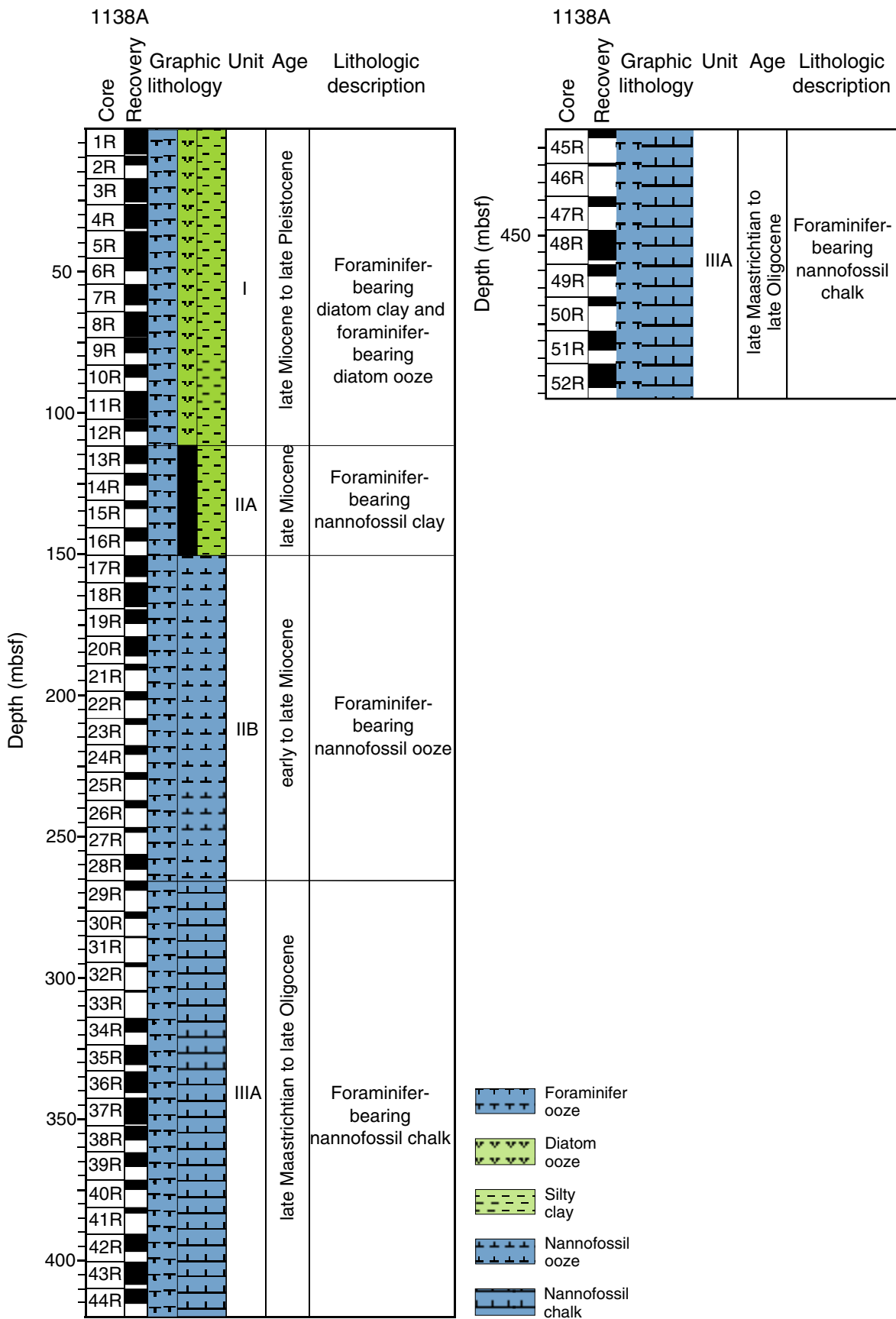


Figure F7. Core photo showing the position of the K/T boundary.

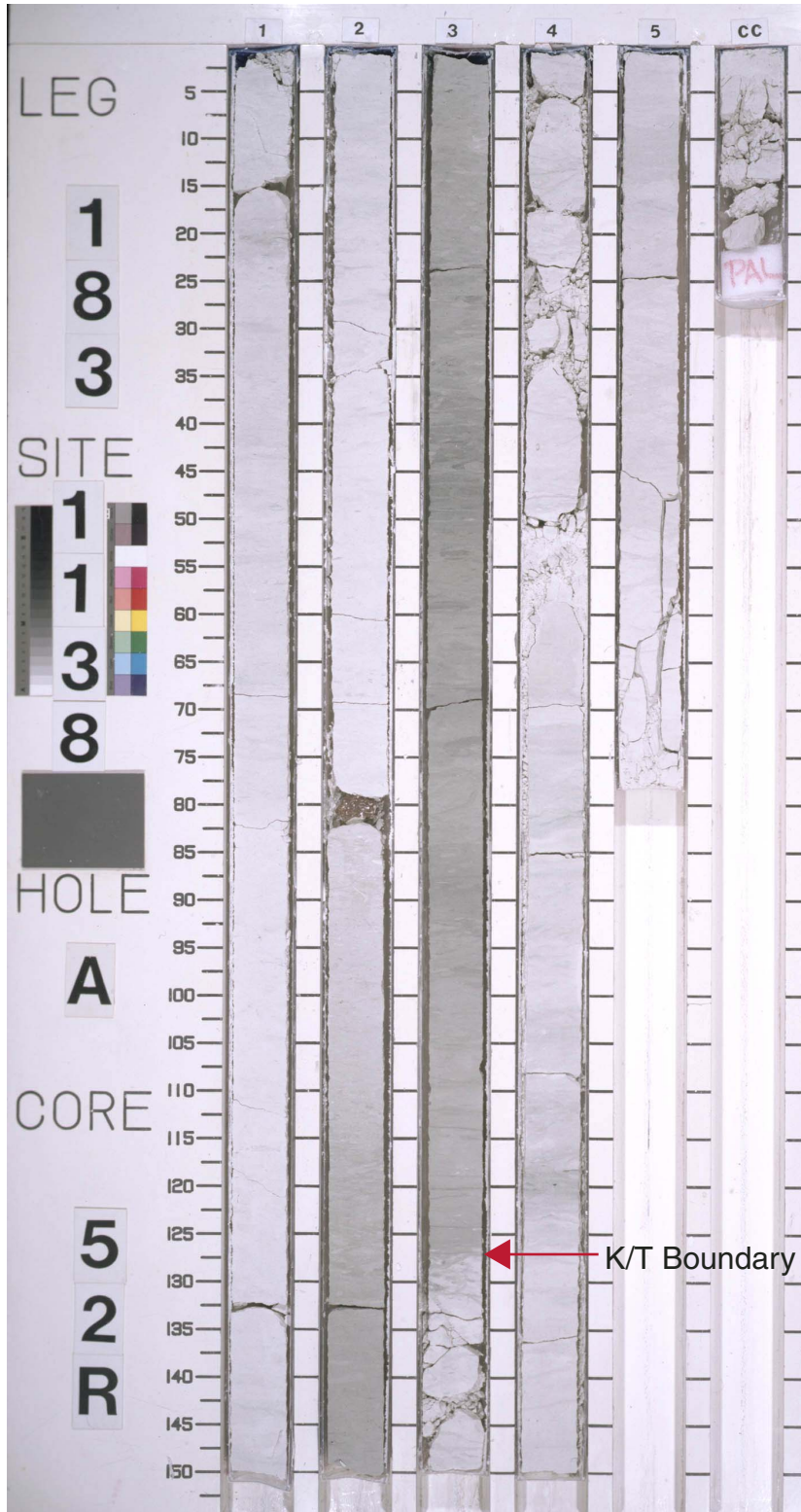


Figure F8. $\delta^{13}\text{C}$ stable isotopic analysis from ODP Site 1138 across the K/T boundary.

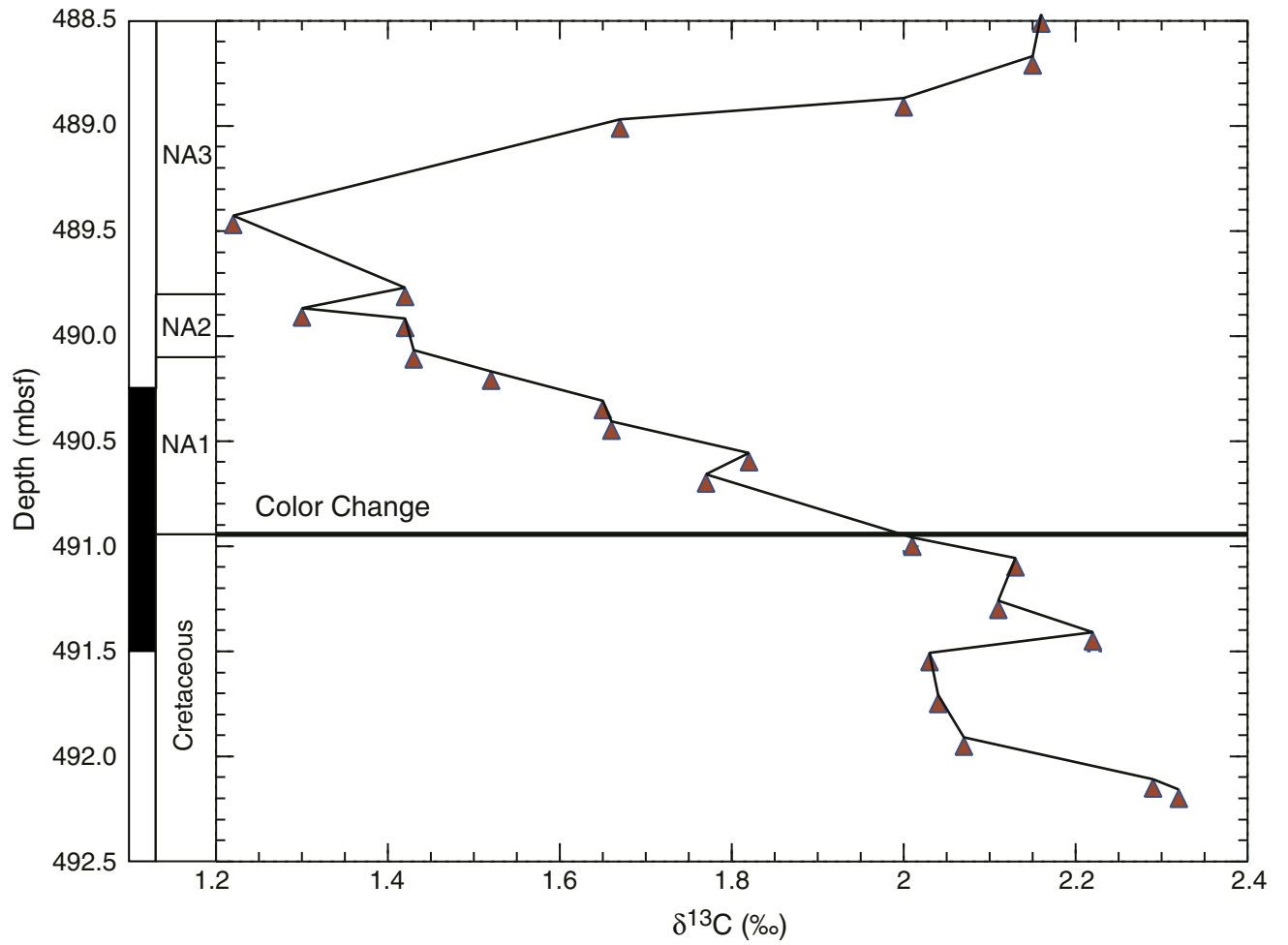


Figure F9. Age-depth plot for Hole 1135A. Comparison slopes are given in the inset box. Pairs of opposed triangles indicate the error bars each nannofossil datum used (see Table T4, p. 47).

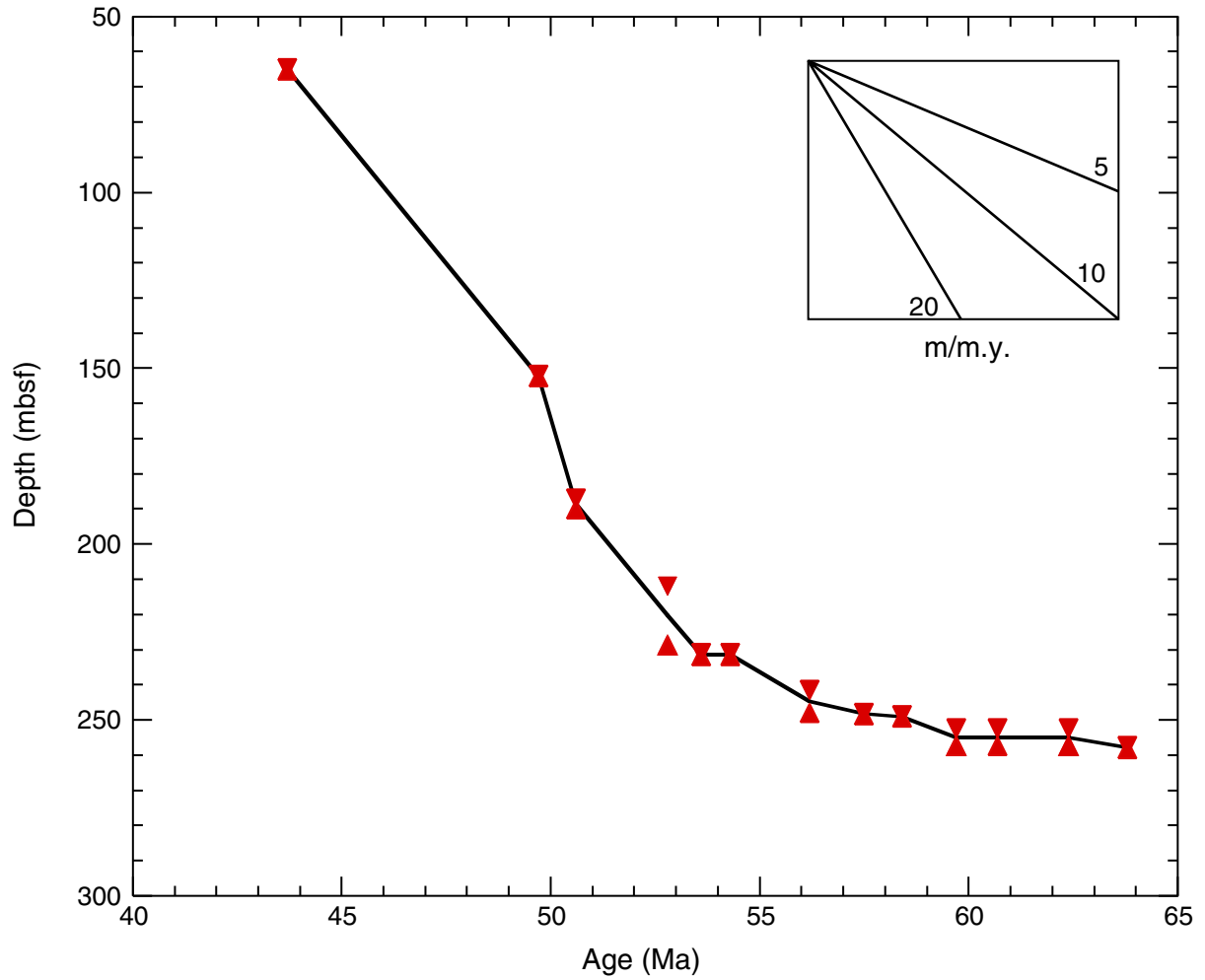


Figure F10. Age-depth plot for Hole 1136A. Comparison slopes are given in the inset box. Pairs of opposed triangles indicate error bars for each nannofossil datum used (see Table T5, p. 49).

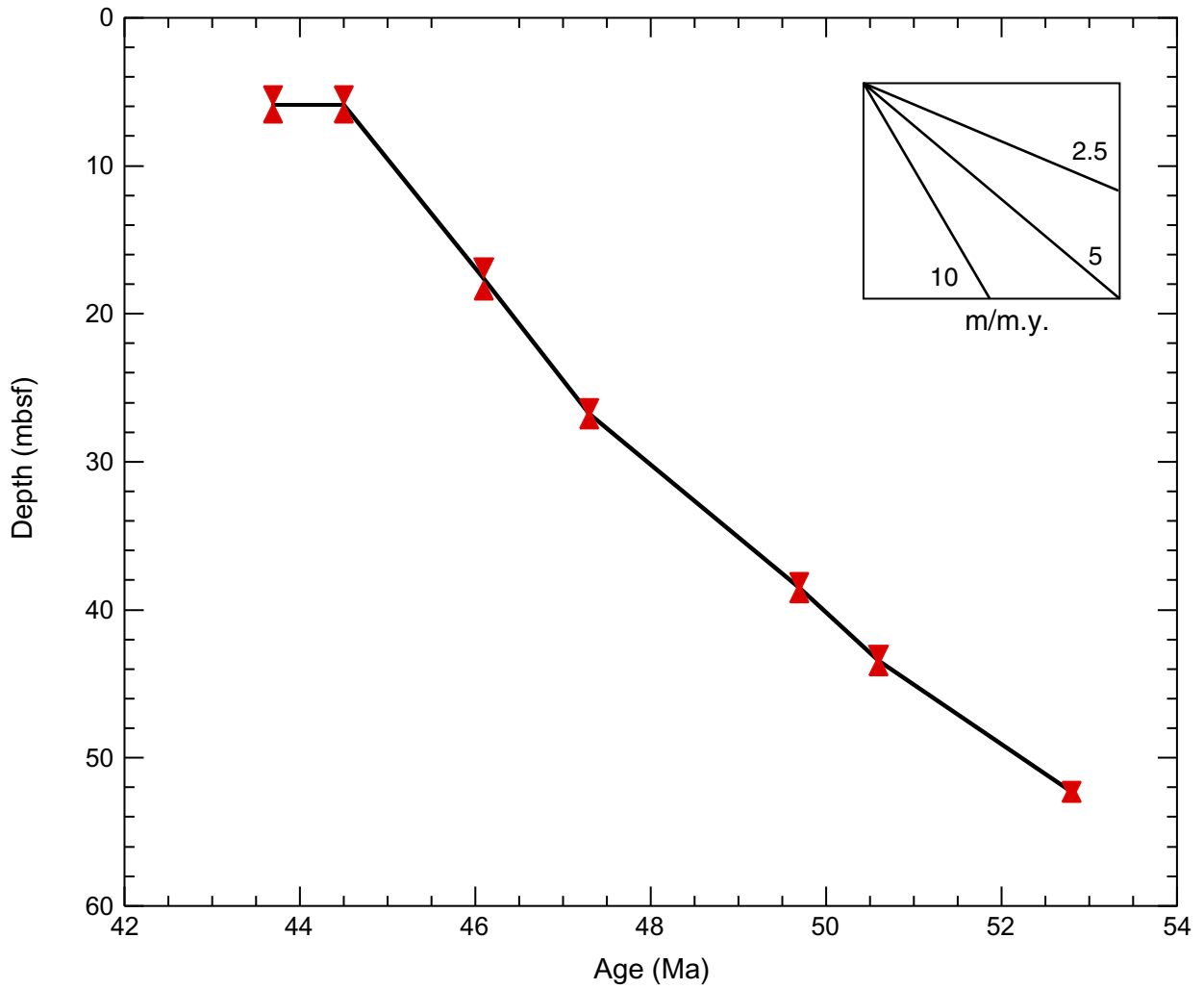


Figure F11. Age-depth plot for Hole 1138A. Comparison slopes are given in the inset box. Pairs of opposed triangles indicate the error bar for each nannofossil datum used (see Table T6, p. 50).

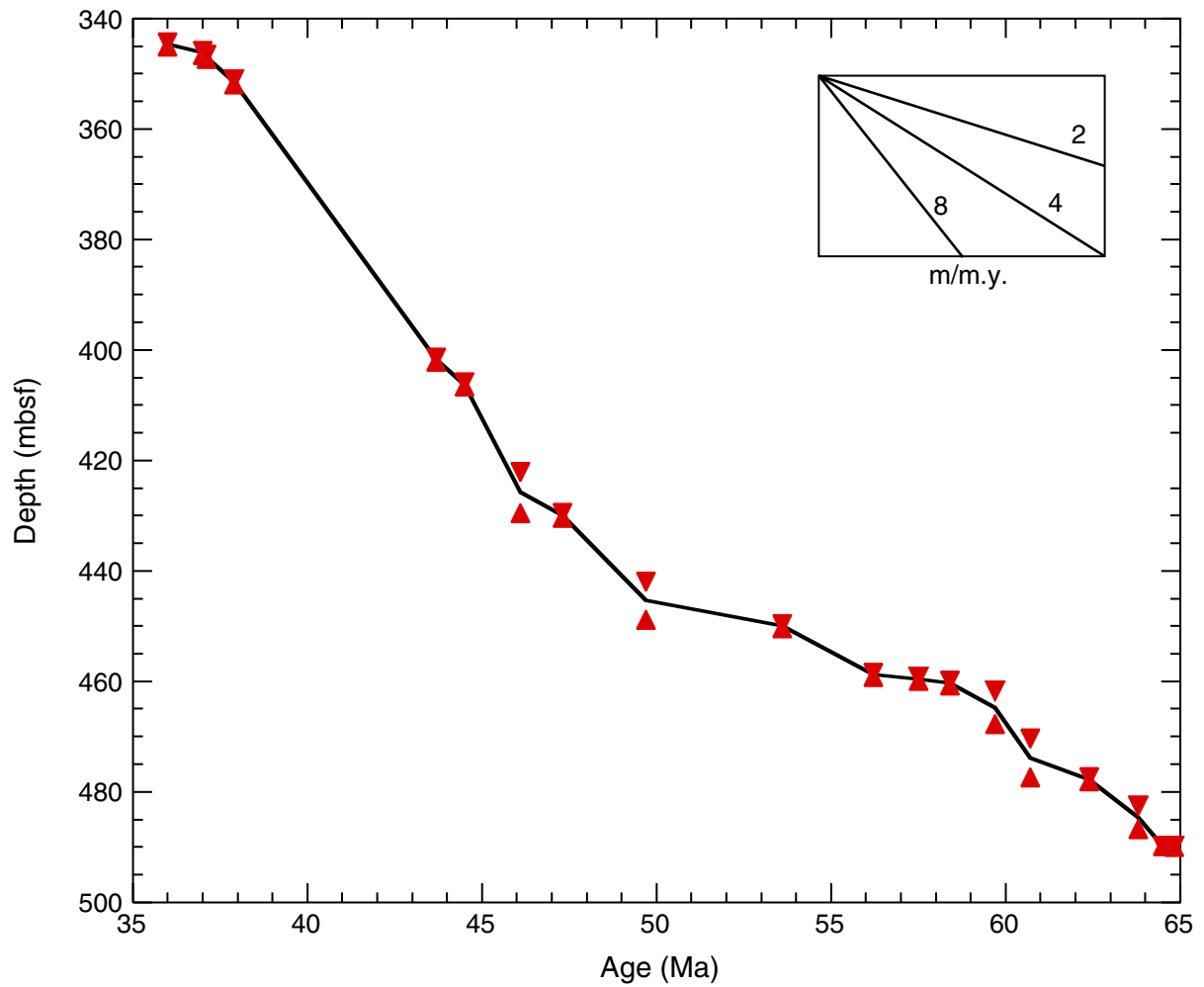


Figure F12. Graphic correlation of ODP Sites 1135, 1136, and 1138.

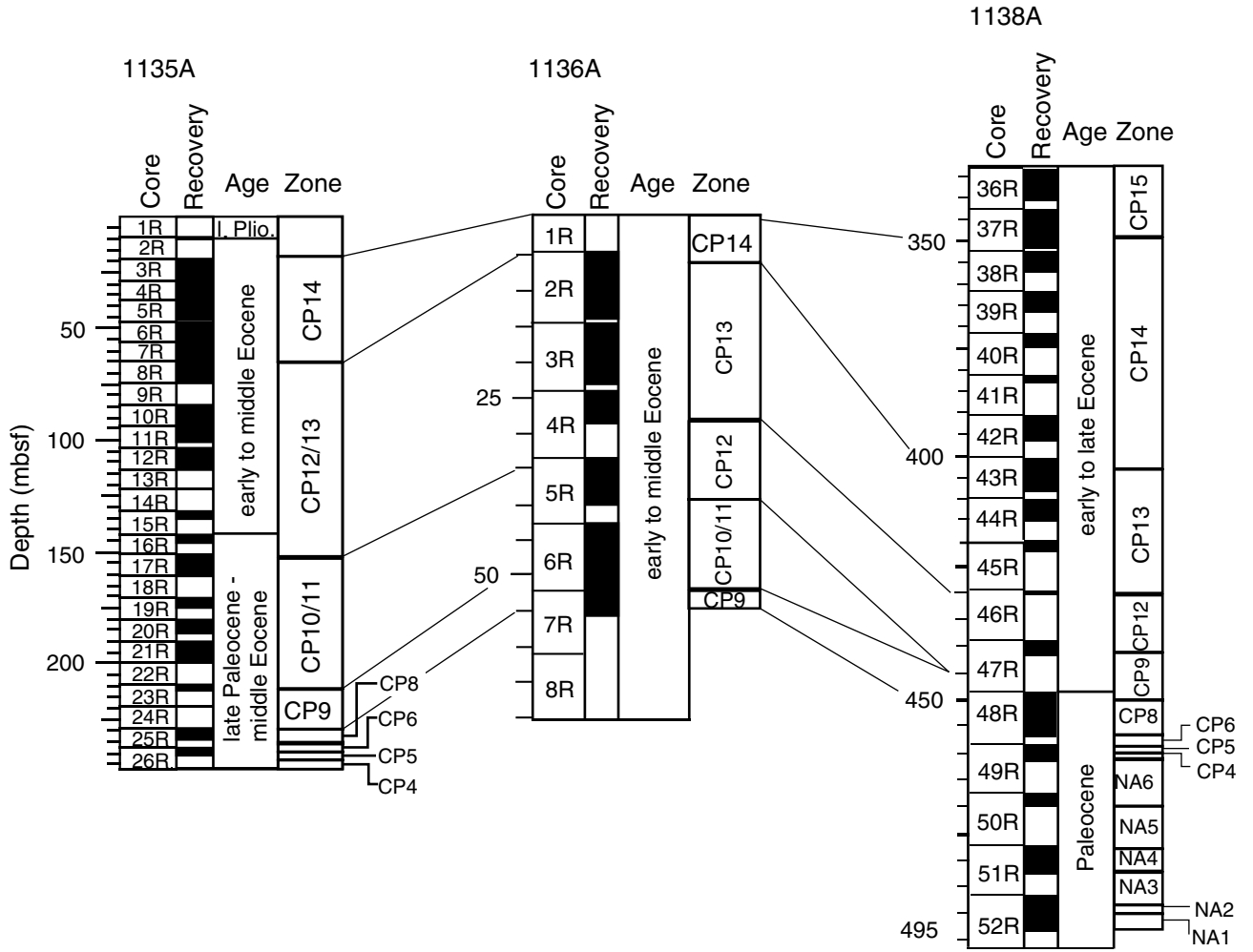


Figure F13. Summary of various carbon isotope curves from around the world compared to Site 1138, (after Pospichal 1996a; Keller and Lindinger, 1989; Shackleton and Hall, 1984; Zachos et al. 1992; Stott and Kennett, 1990). CKP = central Kerguelen Plateau, KP = Kerguelen Plateau, PDB = Peedee belmenite. (Continued on next page.)

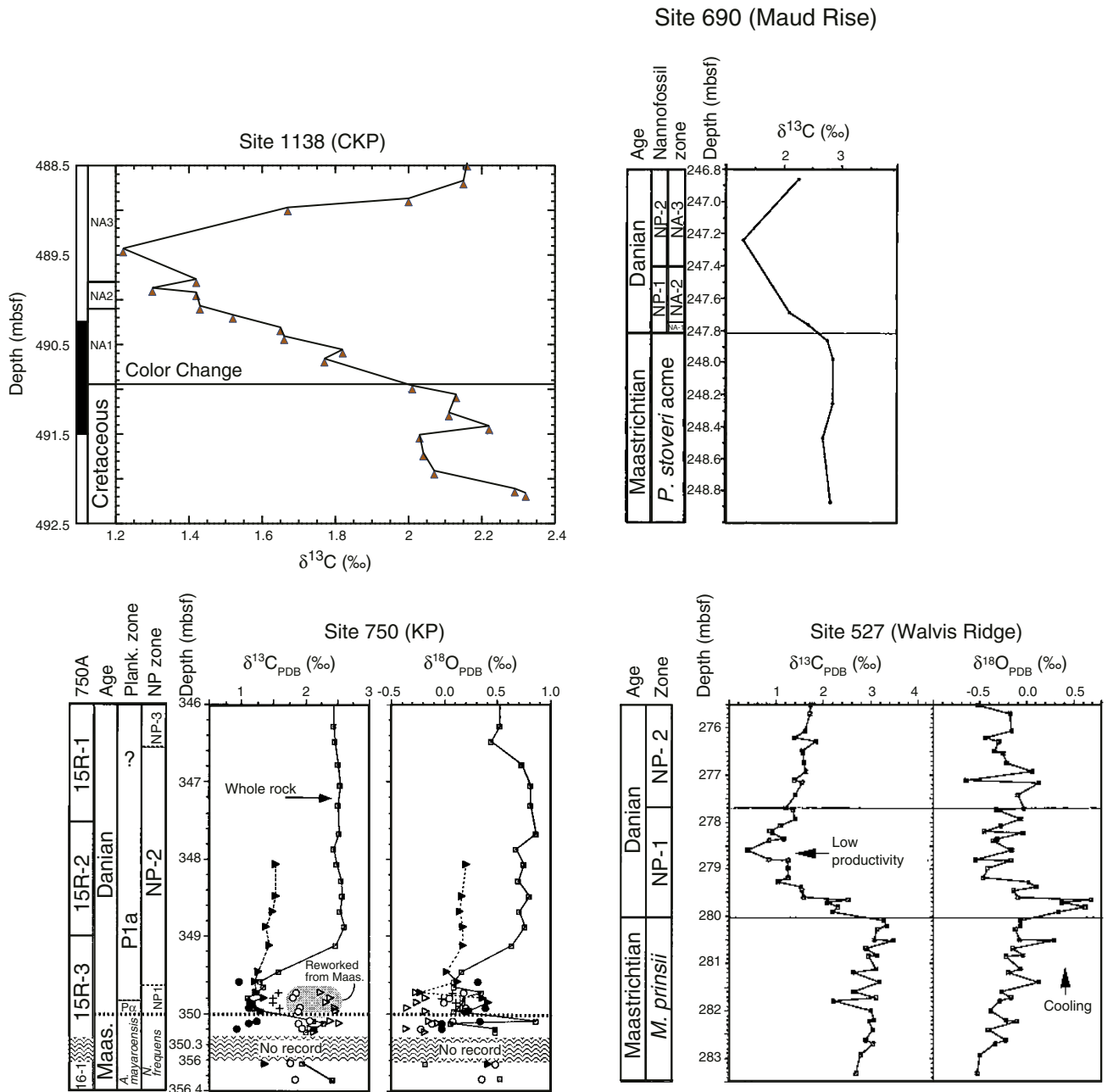


Figure F13 (continued).

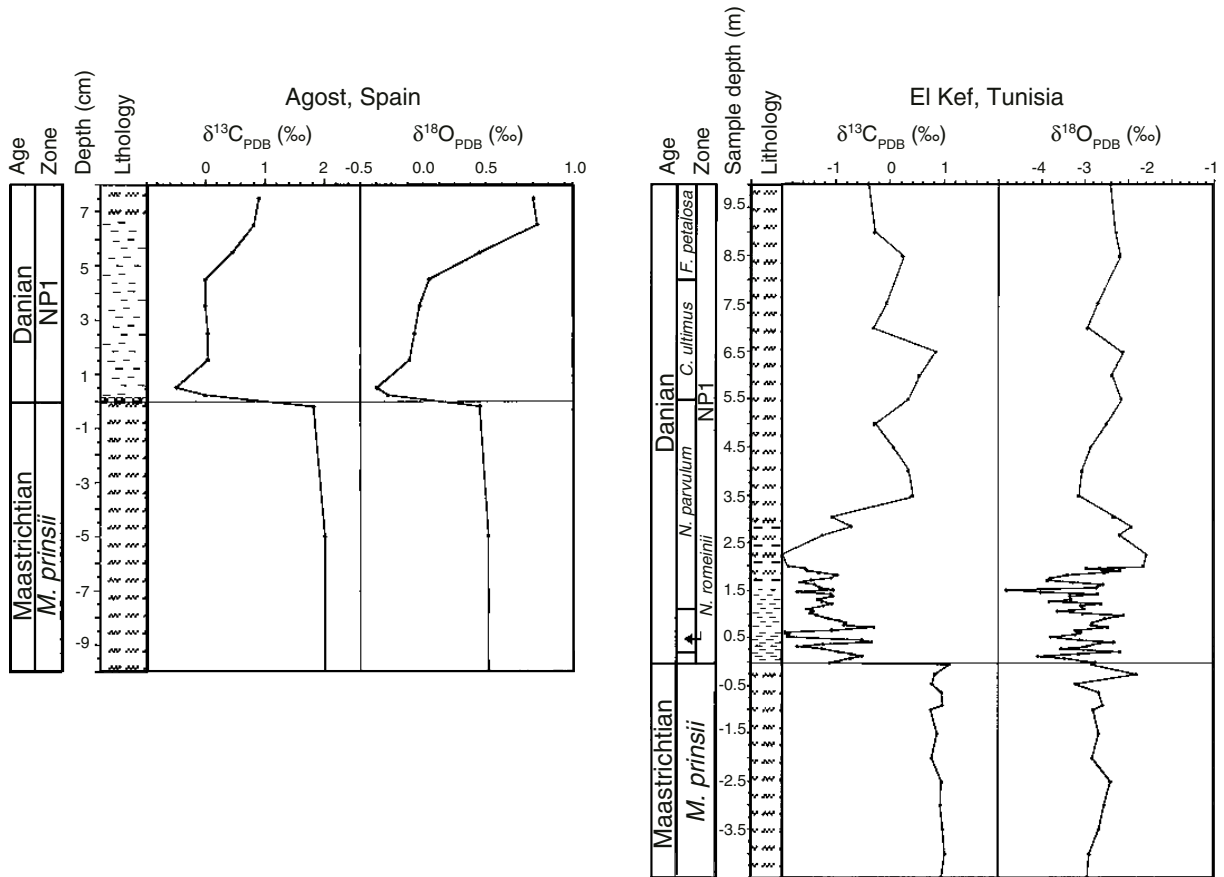


Figure F14. Biogeography of genus *Hornibrookina* in the early Paleocene. (Note: position of Site 752 is at its approximate paleolatitude for this time).

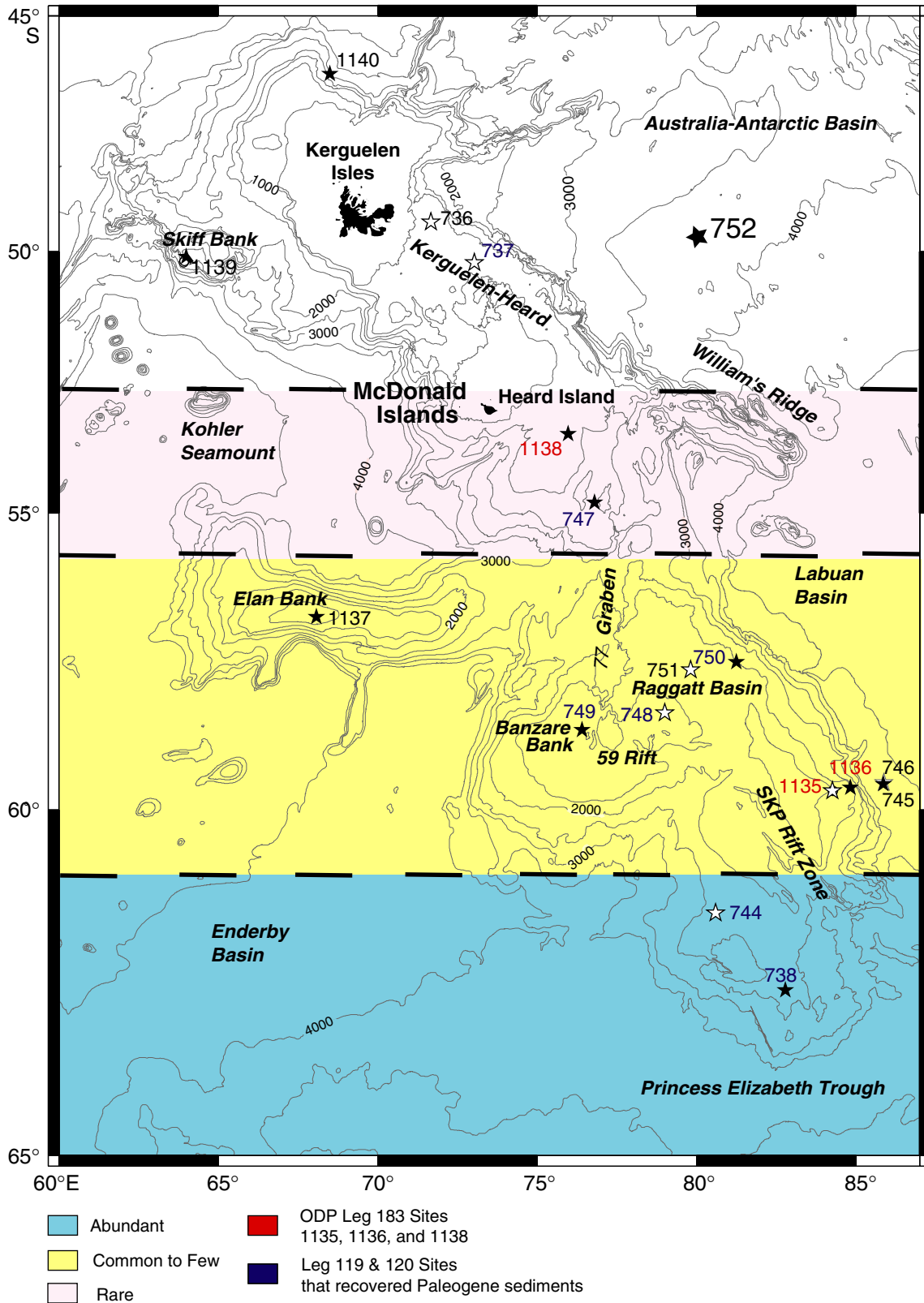


Table T1. Stratigraphic distribution of calcareous nannofossil taxa, Hole 1135A. (This table is available in an [oversized format](#).)

Table T2 (continued).

Age	Zonation (Okada and Bukry, 1980/ Wei and Pospichal, 1991)	Core, section, interval (cm)	Depth (mbsf)	Abundance	Preservation	<i>Neococcolithes minutus</i>	<i>Portosphaera</i> spp.	<i>Pseudotriquetra inversus</i>	<i>Reticulalenestra onusta</i>	<i>Reticulalenestra samodurovi</i>	<i>Reticulalenestra</i> spp.	<i>Reticulalenestra umbilica</i>	Reworked Cretaceous	<i>Sphenolithus moriformis</i>	<i>Sphenolithus radians</i>	<i>Thorasphaera</i> spp.	<i>Toweius?</i> <i>crassus</i>	<i>Toweius magnacrassus</i>	<i>Toweius</i> spp.	<i>Tribrachiatulus orthostylus</i>	<i>Zygrabliothus bijugatus</i>	
middle Eocene	CP14	183-1136A- 2R-1, 58-59	5.28	A M	C			F	F	A	F	F									C	
	CP13b	2R-2, 25-26	6.45	A M	F			F	F	A	F	F				F						C
		2R-6, 35-36	12.55	A M	F			C	C	A		C										C
		2R-6, 100-101	13.2	A M	F			C	F	A												A
		2R-7, 26-27	13.96	A M				F	C	A		F					F					A
		2R-CC	14.28	A M	F			F	C	A		R					F					A
		3R-1, 25-26	14.65	A M	C			F	C	A							F					A
		3R-1, 100-101	15.4	A M	C	R				A	A						F					C
		3R-2, 25-26	16.15	A M						C	A		C				F					A
		3R-2, 100-101	16.9	A M	C					C	A		F				R					C
		3R-3, 100-101	18.4	A M	C					F	A						F					A
		3R-4, 25-26	19.15	A M	C					F	A		F									A
		3R-4, 100-101	19.9	A M	C				F	F	A		C									A
	CP13a	3R-5, 25-26	20.65	A M	F				F	A		C										A
		3R-5, 100-101	21.40	A M	F				C	A		C										A
		3R-6, 25-26	22.15	A M						C	A		F									A
		3R-6, 100-101	22.9	A M	F				C	C	A											A
		3R-CC	23.14	A M	F				C	C	A		F									A
		4R-1, 25-27	24.15	A M	C			R	C	F	A		C				F					A
		4R-1, 100-101	24.9	A M	F				C	F	C		F									A
		4R-2, 25-27	25.65	A M	F				F	F	C		F									A
		4R-2, 100-101	26.4	A M					F	F	C											A
		4R-3, 25-27	27.15	A M						F	C		R									A
		4R-CC	27.67	A M	F					C	A		F						R			C
early Eocene		CP12	5R-1, 100-101	34.4	A M	F				F	A		C									C
	5R-3, 25-26		36.65	A M	C				C	C		C	F		F	F	F	F			A	
	5R-3, 100-101		37.40	A M	F				F	C		C	R		F	F	F	F			A	
	5R-4, 25-26		38.15	A M	F				F	C		C	R		F	F	F	F			A	
	CP10/ CP11	5R-4, 100-101	38.90	A M	F					C		F	F		F	F	F	F				A
		5R-5, 25-26	39.65	A M	F	R				A		F	F		C	F	C	C				A
		5R-CC	39.99	A M	F					C		C	F		F	F	F	F				A
		6R-1, 25-26	43.05	A M	F					C		A	C		F	A	C	F				A
		6R-1, 100-101	43.80	A M	C				F	A		C	C		C	C	F	C	C	R		A
		6R-2, 33-034	44.63	A M	F					C		C			C	C	C	F		A		C
		6R-2, 115-116	45.45	A M	F					F	A		C		C	C	F	F		C		A
		6R-3, 25-26	46.05	A M	C					F	A		C	F	C	C	F	C				A
		6R-3, 100-101	46.80	A M						F	C		C	F	C	C	F	C				A
		6R-4, 25-26	47.55	A M						F	C		C		F	F	C					C
		6R-4, 100-101	48.30	A M						C			R	F	C							A
		6R-5, 25-026	49.05	A M						C			C		C				R		R	A

Table T2 (continued).

Age	Zonation (Okada and Bukry, 1980/ Wei and Pospichal, 1991)	Core, section, interval (cm)	Depth (mbsf)	Abundance		Preservation																
				A	M																	
early Eocene	CP10/ CP11	6R-5, 100–101	49.80	A	M																	
		6R-6, 100–101	51.30	A	M																	
		6R-7, 25–026	52.05	A	M																	
		6R-CC	52.26	A	M																	
		7R-1, 25–026	52.35	A	M																	
		7R-1, 100–101	53.10	A	M																	
	CP9b	7R-2, 25–26	53.85	A	M																	
		7R-2, 100–101	54.60	A	M																	

Notes: Preservation: M = moderate. Abundance: V = very abundant, A = abundant, C = common, F = few, R = rare, B = barren.

Table T2 (continued).

Age	Zonation (Okada and Bukry, 1980/ Wei and Pospichal, 1991)	Core, section, interval (cm)	Depth (mbsf)	Abundance		Preservation	<i>Neococcolithes minutus</i> <i>Portosphaera</i> spp. <i>Pseudotriquetra inversus</i> <i>Reticulalenestra onusta</i> <i>Reticulalenestra samodurovi</i> <i>Reticulalenestra</i> spp. <i>Reticulalenestra umbilica</i> Reworked Cretaceous <i>Sphenolithus moriformis</i> <i>Sphenolithus radians</i> <i>Thoracosphaera</i> spp. <i>Toweius?</i> <i>crassus</i> <i>Toweius magnacrassus</i> <i>Toweius</i> spp. <i>Tribrachiatulus orthostylus</i> <i>Zygrabliithus bijugatus</i>						
				A	M								
early Eocene	CP10/ CP11	6R-5, 100-101	49.80	A	M		F	A	R		R	A	
		6R-6, 100-101	51.30	A	M	F	C	C	C	F	F	A	
		6R-7, 25-026	52.05	A	M	C	C	C	F			R	A
		6R-CC	52.26	A	M	F	C	C	F	C		R	A
		7R-1, 25-026	52.35	A	M		C	C	C	A	C	C	F
	CP9b	7R-1, 100-101	53.10	A	M		C	C	F	A	C	F	A
		7R-2, 25-26	53.85	A	M		C	F	C	C		F	A
		7R-2, 100-101	54.60	A	M	F	F	F	F	C		F	A

Table T3. Stratigraphic distribution of calcareous nannofossil taxa, Hole 1138A. (This table is available in an [oversized format](#).)

Table T4. Nannofossil counts across the K/T boundary, Site 1138. (Continued on next page.)

Age	Nannofossil zonation (Wei and Pospichal, 1991)	Core, section, interval (cm)	Depth (mbsf)	Abundance	Preservation	<i>Acuturis scotus</i>	<i>Almuellerella octoradiata</i>	<i>Arkhangel'skiella cymbiformis</i>	<i>Braarudosphaera bigelowii</i>	<i>Biscutum dissimilis</i>	<i>Biscutum</i> spp.	<i>Chiastozygus amphipons</i>	<i>Chiastozygus garrisonii</i>	<i>Chiastozygus</i> sp.	<i>Cribozentrum daniae</i>	<i>Cribo-sphaerella ehrenbergii</i>	<i>Eiffelithus turrisseiffelii</i>	<i>Eiffelithus</i> sp.	<i>Gartnerago</i> sp.	<i>Kamptnerius magnificus</i>	<i>Lucianorhabdus cayeuxii</i>	<i>Microrhabdulus decoratus</i>	<i>Micula decussata</i>	<i>Misceomarginatus pleniporus</i>	<i>Monomarginatus quaternarius</i>	<i>Nephrolithus miniporus</i>	<i>Nephrolithus frequens</i>	<i>Nephrolithus</i> sp.	<i>Prediscosphaera cretacea</i>	<i>Prediscosphaera</i> spp.	<i>Prediscosphaera spinosa</i>	<i>Prediscosphaera stoveri</i>	<i>Retacapsa crenulata</i>	<i>Reinhardtites anthophorus</i>	<i>Watznaueria barnesae</i>	<i>Zygodiscus compactus</i>	<i>Zygodiscus spiralis</i>	<i>Biscutum constans</i>	<i>Cyclagelosphaera reinhardtii</i>	<i>Lapideacassis</i> sp.	
early Paleocene	NA3	183-1138A-52R-3, 4-4	489.74	A	M	23	1	6			4		4				1	46			1	3				4	11	1	3	3	1	16	3	1			3	11	1		
	NA2	52R-3, 10-011	489.80	A	M	27		7	1			2		5		2		4	1	26		3	1	7			4	7	5	7	6		35	2				3	13		
		52R-3, 20R-22	489.91	A	M	19	4	11				2		2		3		2	40			3	12				4	9	6	4	6		39			1		1	16	1	
	NA1	52R-3,29-29	489.99	A	M	29	4	8				2		5		2		1	46			2	3				4	10	5	6	6	3	30	2		1		2	9	2	
		52R-3,40-42	490.11	A	M	34		9	1			2		3		1	2	2	41				2	12		1	5	8	8	7	12	1	41	3		1		3	9	1	
		52R-3,50-51	490.20	A	M	30	2	10				3		2		6	1	2	36				2	16			5	8	7	7	6	1	56	1				1	9		
		52R-3, 60-60	490.30	A	M	43	3	20				2		4		2		4	38			1	1	9			7	4	6	4	10		44	3		2		1	11		
		52R-3,64-65	490.35	A	M	59		19				3		1		1		4	64			2	3	25	1		3	3	2	9	12		21	2				1	5		
		52R-3,70-070	490.40	A	M	41	1	17				1				1	1	1	44			1	4	17			4	8	7	6	6		39	6		1		13		1	
		52R-3, 75-76	490.45	A	M	43	1	10				2	4			1	6	45				4	4	10			5	10	6	11	9		38	1		1		6	3		
		52R-3, 80-80	490.50	A	M	21	2	13				1	2			1	1	4	51			2	2	21			3	6	8	9	3	1	65			1		13			
		52R-3, 90-91	490.60																																						
		52R-3, 99-99	490.69	A	M	53	1	17				1		3		2	1	52			3	2	29	2			1	6	7	14	8		47	4		2		12			
	52R-3, 109-109	490.79	A	M	45	9	15				2		2		2		1	39			3	2	32			4	7	15	12	5		58	2	2	1		7	1			
	52R-3, 120-120	490.90	A	M	57	2	15				1		1		2	4	1	46			4	2	33			2	6	11	6	12		45			1		2	14			
	52R-3, 127-127	490.97	A	P	55	1	28				2				4	1	48					5	47					8	9	24		23			1		9	2			
	late Maastrichtian	NC23	52R-3, 129-129	490.99	A	P	28		50			2		4		2	3		5	52		1	13				2	6	12	17	15		64	6		2		1	1		
			52R-3, 130-131	491.01	A	M	15	8	26			6		6	8	1	3	2	32			2	5				5	18	16	17	4		113	8				3			
52R-3, 140-141			491.11	A	G	13	10	21			1	8		6	6	2	1	2	21			7	2				11	15	19	14	5		121	7		1		3	1		
52R-4, 10-11			491.31	A	G	13	11	38	2		5		2	6	2		2	24				7	14				5	49	1	14	1		93	2		5		4			

Notes: Preservation: G = good, M = moderate, P = poor. Abundance: A = abundant.

Table T5. Summary of bulk carbonate isotopic values, Site 1138.

Core, section, interval (cm)	Depth (mbsf)	$\delta^{13}\text{C}$ (‰)
183-1138A-		
52R-2, 30–31*	488.51	2.16
52R-2, 50–51*	488.71	2.15
52R-2, 70–71*	488.91	2.00
52R-2, 81–82*	489.01	1.67
52R-2, 127–128*	489.47	1.22
52R-3, 10–11*	489.81	1.42
52R-3, 20–22*	489.91	1.30
52R-3, 25–27*	489.96	1.42
52R-3, 40–42*	490.11	1.43
52R-3, 50–51*	490.21	1.52
52R-3, 64–65*	490.35	1.65
52R-3, 75–76*	490.45	1.66
52R-3, 90–91*	490.60	1.82
52R-3, 100–102*	490.70	1.77
52R-3	491.00	2.01
52R-3, 140*	491.10	2.13
52R-4, 10*	491.30	2.11
52R-4, 25–27*	491.45	2.22
52R-4, 35*	491.55	2.03
52R-4, 55*	491.75	2.04
52R-4, 75*	491.95	2.07
52R-4, 95*	492.15	2.29
52R-4, 100–102*	492.20	2.32

Note: * = bulk sample.

Table T6. Calcareous nannofossil events, Site 1135.

Event	Core, section, interval (cm)		Depth (mbsf)	Age (Ma)
	Top	Bottom		
	183-1135A-	183-1135A-		
FCO <i>Reticulofenestra umbilica</i>	7R-6, 100–101	7R-7, 25–26	64.98	43.7
FO <i>Discoaster subloboensis</i>	17R-1, 25–26	17R-1, 100–101	152.22	49.7
LO <i>Tribrachiatulus orthostylus</i>	20R-CC	21R-1, 25–26	188.61	50.6
FO <i>Discoaster lodoensis</i>	23R-CC	25R-1, 25–26	220.37	52.8
FO <i>Tribrachiatulus orthostylus</i>	25R-2, 100–101	25R-3, 25–26	231.38	53.6
FO <i>Tribrachiatulus contortus</i>	25R-2, 100–101	25R-3, 25–26	231.38	54.3
FO <i>Discoaster multiradiatus</i>	26R-CC	27R-1, 25–26	244.73	56.2
FO <i>Discoaster mohleri</i>	27R-1, 25–26	27R-1, 100–101	248.33	57.5
FO <i>Heliolithus kleinpellii</i>	27R-1, 100–101	27R-2, 25–26	249.08	58.4
FO <i>Fasciculithus tympaniformis</i>	27R-CC	28R-1, 25–26	254.95	59.7
FO <i>Chiasmolithus bidens</i>	27R-CC	28R-1, 25–26	254.95	60.7
FO <i>Prinsius martinii</i>	27R-CC	28R-1, 25–26	254.95	62.4
FO <i>Chiasmolithus danicus</i>	28R-1, 25–26	28R-1, 100–101	257.93	63.8

Notes: Depth is the midpoint between two samples. FO = first occurrence, FCO = first common occurrence, LO = last occurrence.

Table T7. Calcareous nannofossil events, Site 1136.

Event	Core, section, interval (cm)		Depth (mbsf)	Age (Ma)
	Top	Bottom		
	183-1136A-	183-1136A-		
FO <i>Reticulofenestra umbilica</i>	2R-1, 58–59	2R-2, 25–26	5.87	43.7
LO <i>Chiasmolithus gigas</i>	2R-2, 25–26	2R-1, 58–59	5.87	44.5
FO <i>Chiasmolithus gigas</i>	3R-2, 100–101	3R-3, 100–101	17.65	46.1
FO <i>Nannotetrina fulgens</i>	4R-2, 100–101	4R-3, 25–27	26.78	47.3
FO <i>Discoaster subloensis</i>	5R-4, 25–26	5R-4, 100–101	38.53	49.7
LO <i>Tribrachiatulus orthostylus</i>	6R-1, 25–26	6R-1, 100–101	43.43	50.6
FO <i>Discoaster lodoensis</i>	6R-CC	7R-1, 25–26	52.3	52.8

Notes: Depth is the midpoint between two samples. FO = First occurrence, LO = Last occurrence.

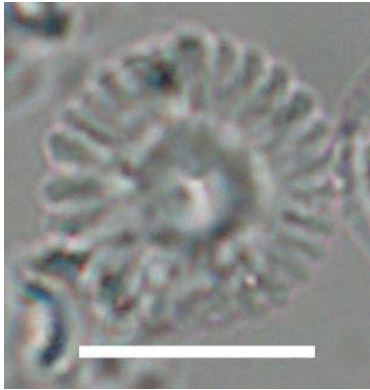
Table T8. Calcareous nannofossil events, Site 1138.

Events	Core, section, interval (cm)		Depth (mbsf)	Age (Ma)
	Top	Bottom		
	183-1138A-	183-1138A-		
FO <i>Isthmolithus recurvus</i>	37R-2, 25–26	37R-2, 100–101	344.73	36
FO <i>Chiasmolithus oamaruensis</i>	37R-3, 25–26	37R-3, 100–101	346.23	37
LO <i>Chiasmolithus grandis</i>	37R-3, 100–101	37R-4, 25–026	346.98	37.1
LO <i>Chiasmolithus solitus</i>	37R-6, 100–101	37R-CC	351.52	37.9
FCO <i>Reticulofenestra umbilica</i>	43R-1, 100–101	43R-2, 25–26	401.78	43.7
LO <i>Chiasmolithus gigas</i>	43R-4, 100–101	43R-5, 25–26	406.28	44.5
FO <i>Chiasmolithus gigas</i>	45R-CC	46R-1, 25–26	425.82	46.1
FO <i>Nannotetrina fulgens</i>	46R-1, 25–26	46R-CC	429.96	47.3
FO <i>Discoaster subloensis</i>	47R-CC	48R-1, 25–26	445.38	49.7
FO <i>Tribrachiatulus orthostylus</i>	48R-1, 100–101	48R-2, 25–26	449.96	53.6
FO <i>Discoaster multiradiatus</i>	49R-1, 25–26	49R-1, 100–101	458.83	56.2
FO <i>Discoaster mohleri</i>	49R-1, 100–101	49R-2, 25–26	459.58	57.5
FO <i>Heliolithus kleinpellii</i>	49R-2, 25–26	49R-2, 100–101	460.33	58.4
FO <i>Fasciculithus tympaniformis</i>	49R-CC	50R-1, 25–26	464.72	59.7
FO <i>Chiasmolithus bidens</i>	50R-CC	51R-1, 25–26	473.89	60.7
FO <i>Prinsius martinii</i>	51R-1, 25–26	51R-1, 100–101	477.73	62.4
FO <i>Chiasmolithus danicus</i>	51R-4, 100–101	52R-1, 3–3	484.29	63.8
FO <i>Cruciplacolithus tenuis</i>	52R-3, 4–4	52R-3, 10–11	489.76	64.5
FO <i>Hornibrookina</i> sp.	52R-3, 29–29	52R-3, 40–42	490.05	64.83

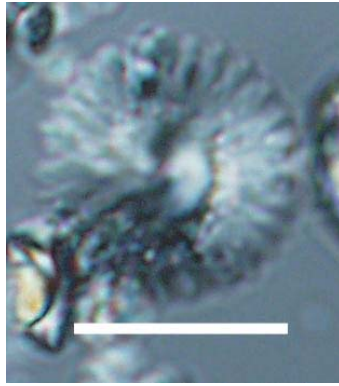
Notes: Depth is the midpoint between two samples. FO = first occurrence, FCO = first common occurrence, LO = last occurrence.

Plate P1. Scale bar = 10 μm . 1A–1B. *Discoaster multiradiatus* (Sample 183-1135A-26R-2, 25–26 cm); (1A) differential interference contrast light (DIC), (1B) transmitted light. 1C. Sample 183-1135A-25R-1, 25–26 (scanning electron microscope [SEM]). 2A, 2B. *Fasciculithus magnicordis* (Sample 183-1135A-26R-2, 25–26 cm); (2A) DIC, (2B) crossed polarizers. 3A–3C. *Neochiastozygus junctus* (Sample 183-1135A-26R-2, 25–26 cm); (3A) DIC, (3B) transmitted light, (3C) crossed polarizers. 3D. *Neochiastozygus junctus* (Sample 183-1135A-25R-1, 25–26 cm; SEM).

1A



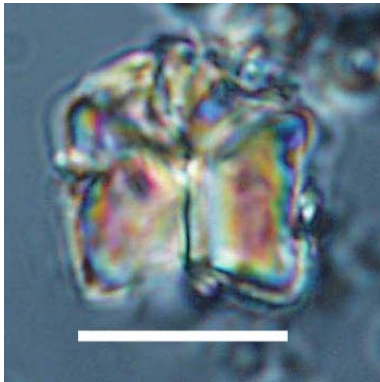
1B



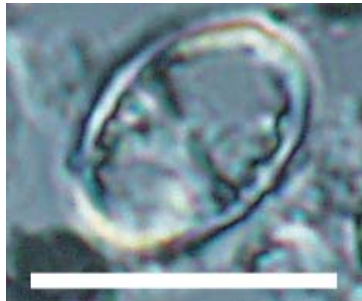
1C



2A



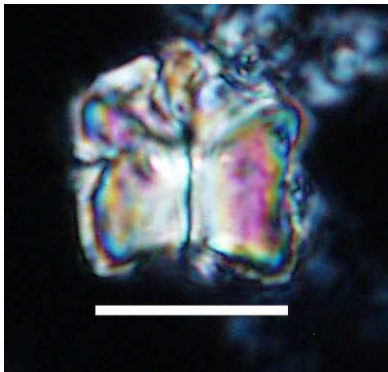
3A



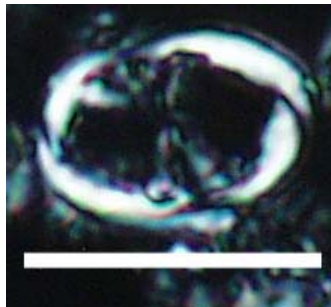
3B



2B



3C



3D

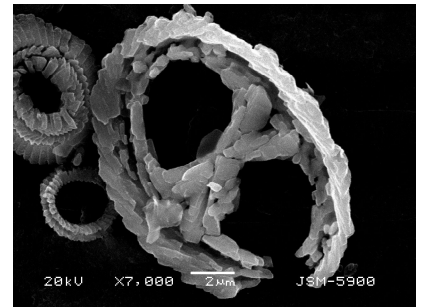
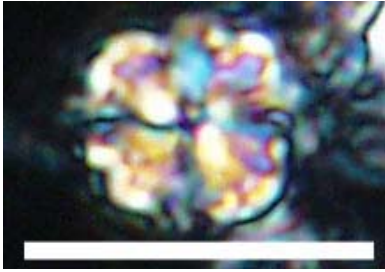
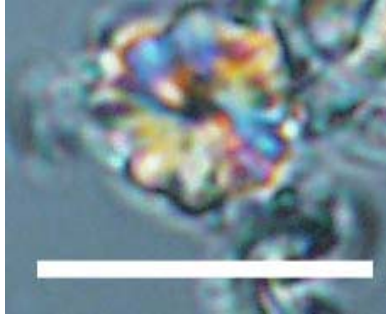


Plate P2. Scale bar = 10 μ m. 1A, 1B. *Fasciculithus* sp. (Sample 183-1135A-26R-2, 25–26 cm); (1A) crossed polarizers, (1B) differential interference contrast light (DIC). 2A, 2B. *Ellipsolithus distichus* (Sample 183-1135A-26R-2, 25–26 cm); (1A) crossed polarizers, (1B) DIC. 3A, 3B. *Fasciculithus tympaniformis* (Sample 183-1135A-26R-2, 25–26 cm); (3A) crossed polarizers, (3B) DIC. 4A–4C. *Toweius pertusus* (Sample 183-1135A-26R-2, 25–26 cm); (4A) DIC, (4B) transmitted light, (4C) crossed polarizers. 5A, 5B. *Neococcolithes dubius* (Sample 183-1138A-44R-4, 25–26 cm); (5A) crossed polarizers, (5B) transmitted light. 5C. *Neococcolithes dubius* (Sample 183-1135A-25R-1, 25–26 cm; scanning electron microscope).

1A



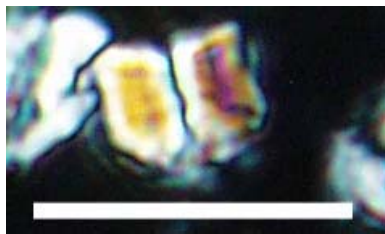
1B



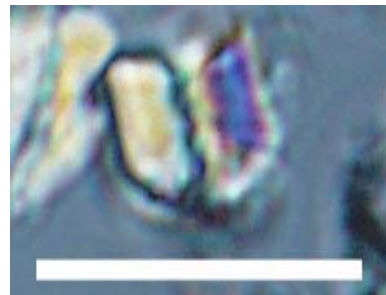
2A



3A



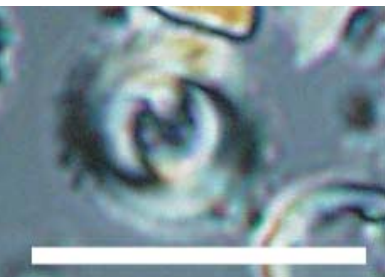
3B



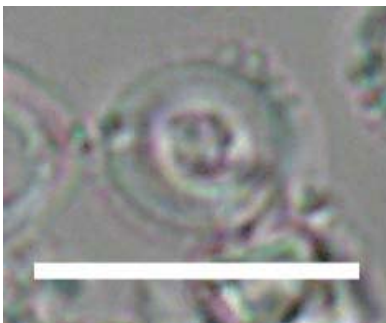
2B



4A



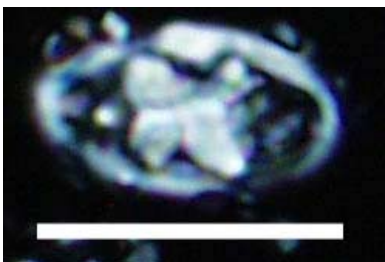
4B



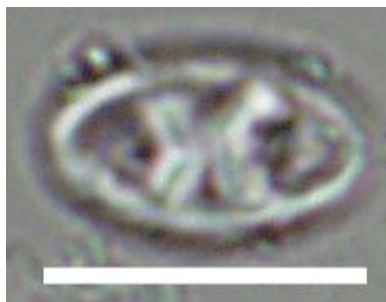
4C



5A



5B



5C

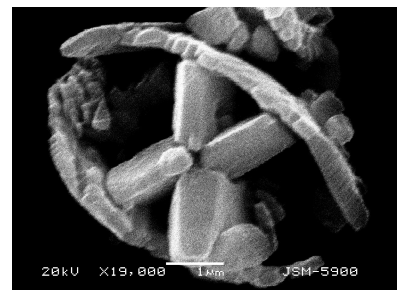
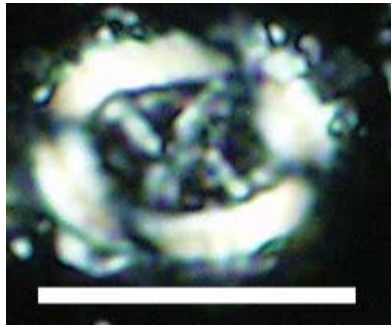


Plate P3. Scale bar = 10 μ m. 1A–1C. *Chiasmolithus danicus* (Sample 183-1135A-27R-3, 96–97 cm); (1A) differential interference contrast light (DIC), (1B) transmitted light, (1C) crossed polarizers. 2A–2C. *Prinsius bisulcus* (Sample 183-1135A-27R-3, 96–97 cm); (2A) DIC, (2B) transmitted light, (2C) crossed polarizers. 3A, 3B. *Prinsius martinii* (Sample 183-1135A-27R-3, 96–97 cm; crossed polarizers). 4. *Nannotetrina fulgens* (Sample 183-1138A-44R-4, 25–26 cm; transmitted light).

1A



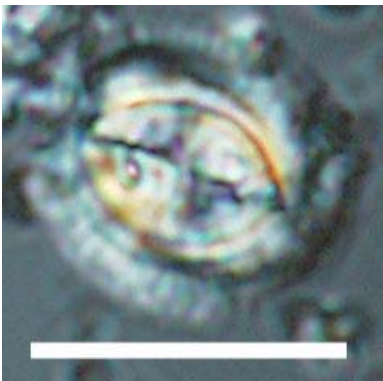
1B



1C



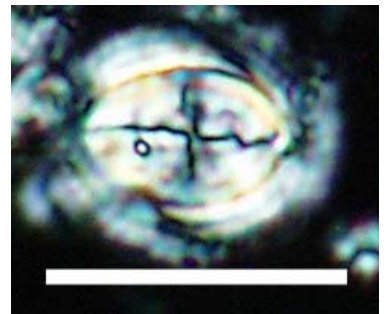
2A



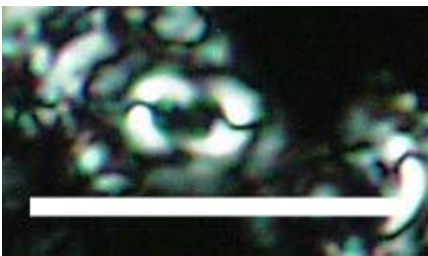
2B



2C



3A



3B



4

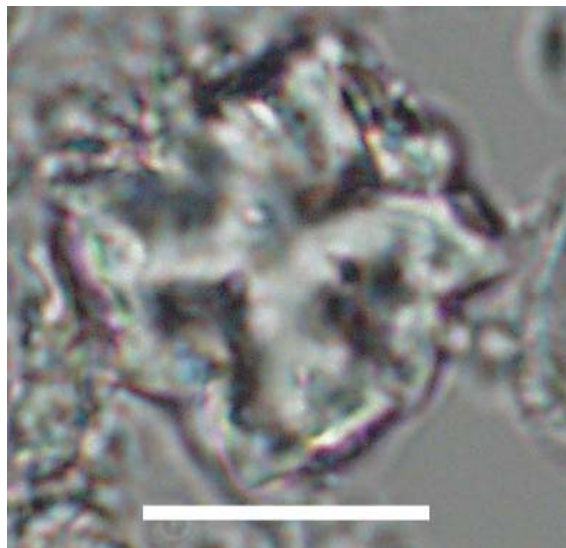


Plate P4. Scale bar = 10 μ m. 1A–AC. *Chiasmolithus oamaruensis* (Sample 183-1138A-37R-1, 25–26 cm); (1A) crossed polarizers, (1B) differential interference contrast light (DIC), (1C) transmitted light. 2A–2C. *Isthmolithus recurvus* (Sample 183-1138A-37R-1, 25–26 cm); (2A) crossed polarizers, (2B) DIC, (2C) transmitted light. 3A, 3B. *Isthmolithus recurvus* (side view) (Sample 183-1138A-37R-1, 25–26 cm); (3A) crossed polarizers, (3B) DIC. 4. *Reticulofenestra umbilica* (Sample 183-1138A-37R-1, 25–26; crossed polarizers). 5A–5C. *Reticulofenestra bisecta* (Sample 183-1138A-37R-1, 25–26 cm); (5A) crossed polarizers, (5B) DIC, (5C) transmitted light.

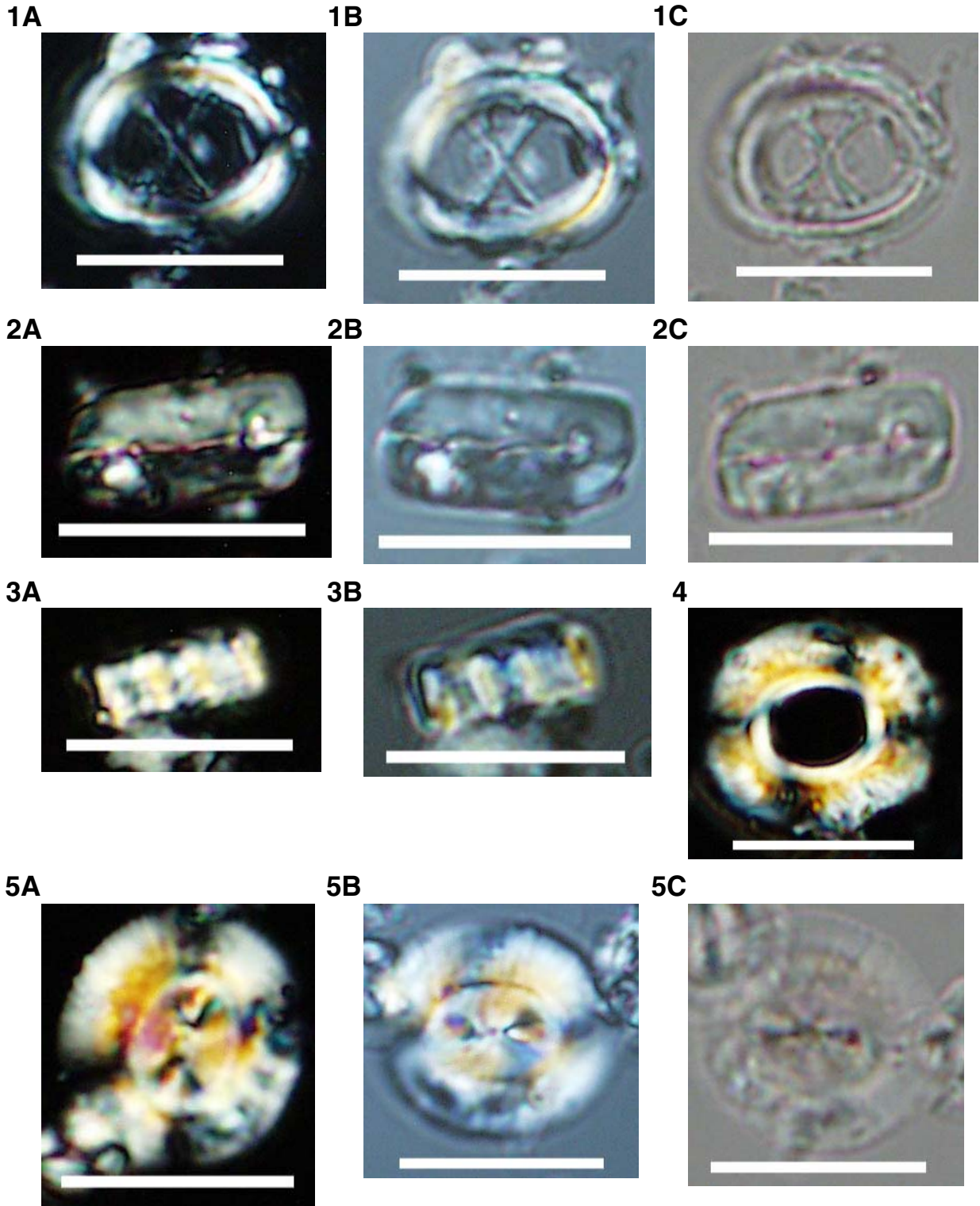
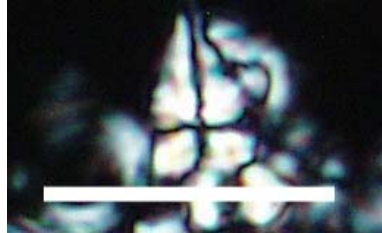


Plate P5. Scale bar = 10 μm . 1A, 1B. *Sphenolithus radians* (Sample 183-1135A-22R-CC; crossed polarizers). 1C, 1D. *Sphenolithus radians* (Sample 183-1135A-20R-4, 100–101 cm; crossed polarizers). 2A, 2B. *Sphenolithus moriformis* (Sample 183-1135A-20R-4, 100–101 cm; crossed polarizers). 3A, 3B. *Tribrachiatus orthostylus* (Section 183-1135A-22R-CC; transmitted light). 4. *Sphenolithus primus* (Sample 183-1135A-25R-1, 25–26 cm; scanning electron microscope).

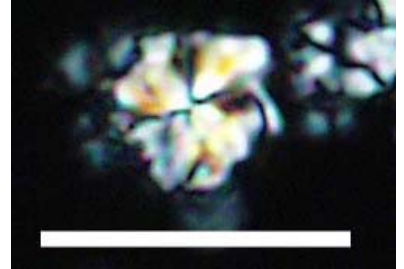
1A



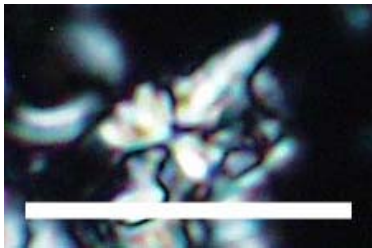
1B



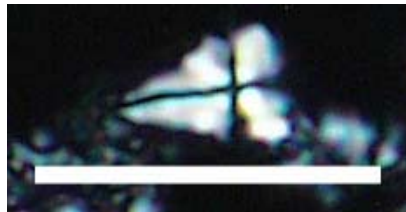
2A



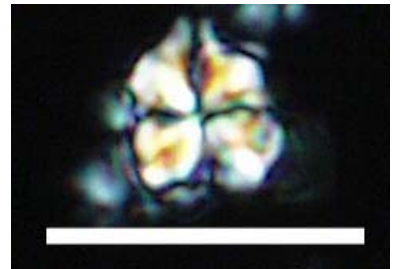
1C



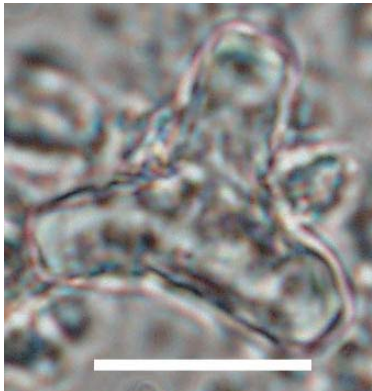
1D



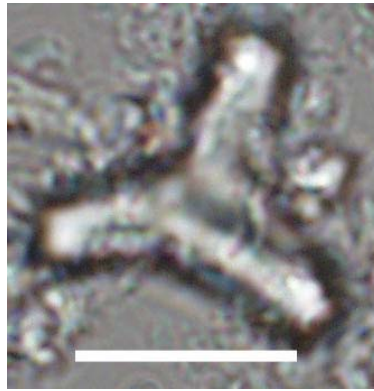
2B



3A



3B

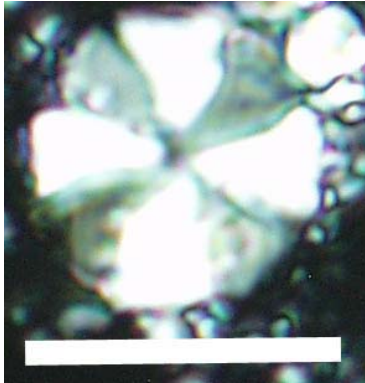


4



Plate P6. Scale bar = 10 μ m. Sample 183-1138A-52R-3, 4 cm. 1A–1C. *Biantholithus sparsus*; (1A) crossed polarizers, (1B) transmitted light, (1C) differential interference contrast light (DIC). 2A, 2B. *Markalius inversus*; (2A) crossed polarizers, (2B) DIC. 3A, 3B. *Placozygus sigmoides*; (3A) crossed polarizers, (3B) DIC. 4A, 4B. *Cruciplacolithus tenuis*; (4A) crossed polarizers, (4B) DIC.

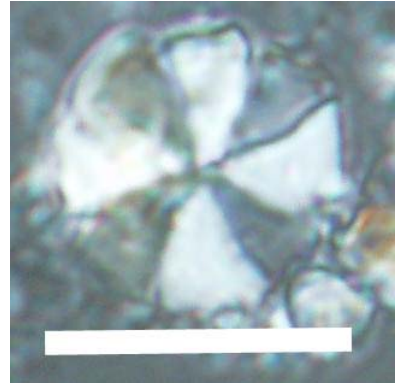
1A



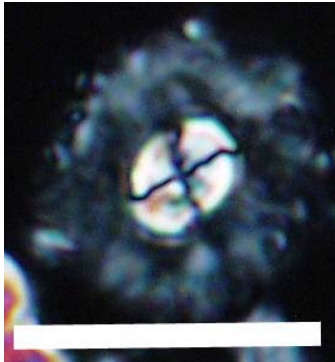
1B



1C



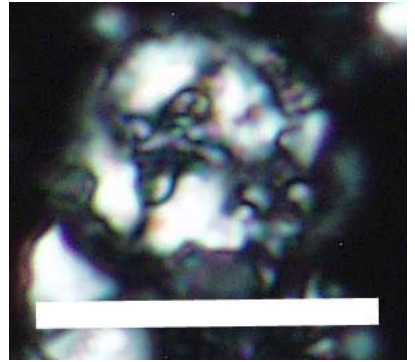
2A



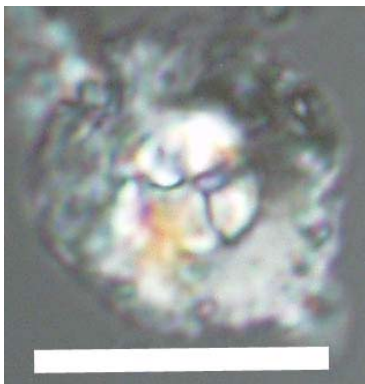
3A



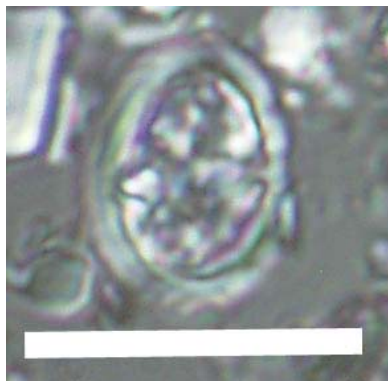
4A



2B



3B

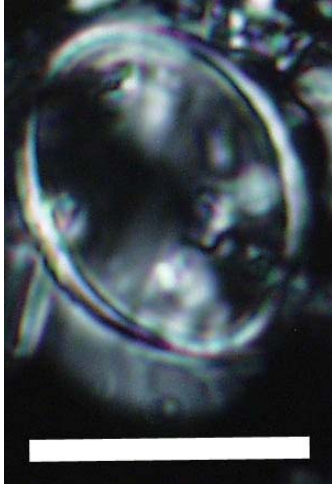


4B



Plate P7. Scale bar = 10 μm . Sample 183-1138A-52R-3, 140–141 cm. 1A–1C. *Kamptnerius magnificus*; (1A) crossed polarizers, (1B) transmitted light, (1C) differential interference contrast light (DIC). 2A–2C. *Nephrolithus frequens*; (2A) crossed polarizers, (2B) transmitted light, (2C) DIC. 3A, 3B. *Arkhangelskiella cymbiformis*; (3A) crossed polarizers, (3B) DIC. 4. *Prediscosphaera cretacea* (crossed polarizers).

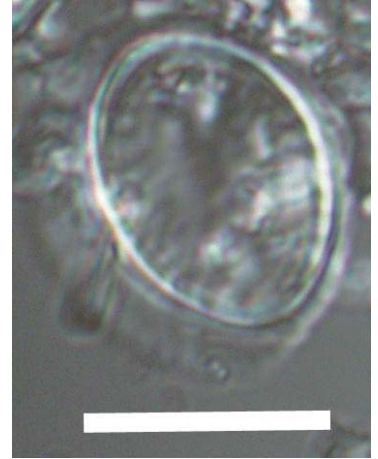
1A



1B



1C



2A



2B



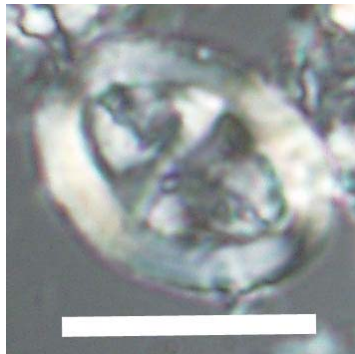
2C



3A



3B



4

